Polymer 54 (2013) 2473–2488

Contents lists available at SciVerse ScienceDirect

Polymer

journal homepage: www.elsevier.com/locate/polymer

Feature article

Amyloids: From molecular structure to mechanical properties

Michael Schleeger [a], Corianne C. vandenAkker [b], Tanja Deckert-Gaudig [c], Volker Deckert [c,d], Krassimir P. Velikov [e,f], Gijsje Koenderink [b], Mischa Bonn [a,*]

[a] Max Planck Institute for Polymer Research, Department of Molecular Spectroscopy, Ackermannweg 10, 55128 Mainz, Germany
[b] FOM Institute AMOLF, Science Park 104, 1098 XG, Amsterdam, The Netherlands
[c] Institute of Photonic Technology, Albert-Einstein-Str. 9, 07745 Jena, Germany
[d] Institute for Physical Chemistry & Abbe School of Photonics, University of Jena, Helmholtzweg 4, 07743 Jena, Germany
[e] Unilever R&D Vlaardingen, Olivier van Noortlaan 120, 3133 AT Vlaardingen, The Netherlands
[f] Soft Condensed Matter, Debye Institute for Nanomaterials Science, Department of Physics and Astronomy, Utrecht University, Princetonplein 5, 3584 CC Utrecht, The Netherlands

ARTICLE INFO

Article history:
Received 9 November 2012
Received in revised form
21 January 2013
Accepted 11 February 2013
Available online 4 March 2013

Keywords:
Amyloids
Vibrational spectroscopy
Biopolymers

ABSTRACT

Many proteins of diverse sequence, structure and function self-assemble into morphologically similar fibrillar aggregates known as amyloids. Amyloids are remarkable polymers in several respects. First of all, amyloids can be formed from proteins with very different amino acid sequences; the common denominator is that the individual proteins constituting the amyloid fold predominantly into a β-sheet structure. Secondly, the formation of the fibril occurs through non-covalent interactions between primarily the β-sheets, causing the monomers to stack into fibrils. The fibrils are remarkably robust, considering that the monomers are bound non-covalently. Finally, a common characteristic of fibrils is their unbranched, straight, fiber-like structure arising from the intertwining of the multiple β-sheet filaments. These remarkably ordered and stable nanofibrils can be useful as building blocks for protein-based functional materials, but they are also implicated in severe neurodegenerative diseases. The overall aim of this article is to highlight recent efforts aimed at obtaining insights into amyloid proteins on different length scales. Starting from molecular information on amyloids, single fibril properties and mechanical properties of networks of fibrils are described. Specifically, we focus on the self-assembly of amyloid protein fibrils composed of peptides and denatured model proteins, as well as the influence of inhibitors of fibril formation. Additionally, we will demonstrate how the application of recently developed vibrational spectroscopic techniques has emerged as a powerful approach to gain spatially resolved information on the structure–function relation of amyloids. While spectroscopy provides information on local molecular conformations and protein secondary structure, information on the single fibril level has been developed by diverse microscopic techniques. The approaches to reveal basic mechanical properties of single fibrils like bending rigidity, shear modulus, ultimate tensile strength and fracture behavior are illustrated. Lastly, mechanics of networks of amyloid fibrils, typically forming viscoelastic gels are outlined, with a focus on (micro-) rheological properties. The resulting fundamental insights are essential for the rational design of novel edible and biodegradable protein-based polymers, but also to devise therapeutic strategies to combat amyloid assembly and accumulation during pathogenic disorders.

1. Introduction

Amyloids constitute a fascinating class of biopolymers that consist of non-covalently bound aggregates of misfolded polypeptides, resulting in insoluble fibrous protein aggregates sharing specific structural traits. Amyloids are set apart from other biopolymers such as DNA and polysaccharides, in that the respective monomers of amyloids are comparatively large polypeptides which polymerize to form a so-called cross-β structure. Moreover, the bonds between the monomers are non-covalent. As a result of misfolding, the individual polypeptides constituting an amyloid fibril fold predominantly into a β-sheet structure. The strong, but non-covalent interaction between the β-sheets gives rise to stacking of the peptides into protofibrils, which can subsequently assemble into large fibrils with a diameter of several nm's and a length up to many microns. Many different biological and artificial peptides can form amyloid structures under the right conditions. *In vivo*, amyloids are often associated with neurodegenerative diseases like Alzheimer, diabetes and Parkinson's disease. However both biogenic and artificial amyloids are also widely applied, for instance, in structuring foodstuffs.

* Corresponding author. Tel.: +49 6131 3791 60; fax: +49 6131 379 360.
E-mail address: bonn@mpip-mainz.mpg.de (M. Bonn).

0032-3861
http://dx.doi.org/10.1016/j.polymer.2013.02.029

Amyloid fibrils can be regarded as biopolymers very similar to silk [1], exhibiting common key features: they originate primarily from unstructured precursor proteins and the definition of the materials occurs through its specific structural and mechanical properties rather than through its detailed chemical composition. The cross-β sheet core structure of amyloid fibrils is very rigid and confers superior mechanical properties. The fibrils can exhibit a Young's modulus similar to that of silk [2] and an ultimate strength similar to steel [2,3]. As such, amyloid fibrils constitute promising building blocks for bio-inspired materials. The fibrils form spontaneously from a wide range of natural proteins. The structural and mechanical properties are relatively insensitive to the protein amino acid sequence [4] and to a wide range of chemical and biochemical modifications [5]. The unique structure of amyloid fibrils renders them relatively robust, even under extreme conditions such as high and low temperature, the presence of proteases, detergents and denaturants, and physical forces [6]. The recent increase in research activity in the area of amyloid-based materials [7] is therefore not surprising. Amyloid fibrils have been used as templates for metallic nanowires that could be used for molecular electronics [6], have been proven to be efficient drug delivery vehicles [8] and are useful as scaffolds for tissue engineering [9]. In the context of human diseases (see Section 2), their robustness against chemicals generally impedes effective medical treatment of amyloid-based diseases.

Despite the broad interest in this relatively novel class of materials, a detailed understanding of the relation between the molecular properties of amyloids and their material characteristics like stiffness and mechanical strength has remained challenging. For instance, the high β-sheet content as the main secondary structure characteristic of amyloids is related to their structural stability [3]. But amyloids contain additional secondary structures and exhibit a distinct polymorphism [10–12], seeming to weaken the exclusive role of β-sheets as the determinant of amyloid stiffness and mechanical strength. In particular, the role of the amino acid side chains remains to be elucidated in that context. The lag in our basic understanding of the relation between amyloid structure and mechanical properties may be traced back to the limited number of techniques that can provide information on the molecular interactions underlying the assembly and material properties of protein fibrils. The material properties of amyloids are based on delicately interconnected effects occurring at a variety of length scales, as illustrated in Fig. 1. Our article will highlight recent applications of various techniques aimed at elucidating the molecular structures and mechanical properties of amyloid-fibrils and derived materials.

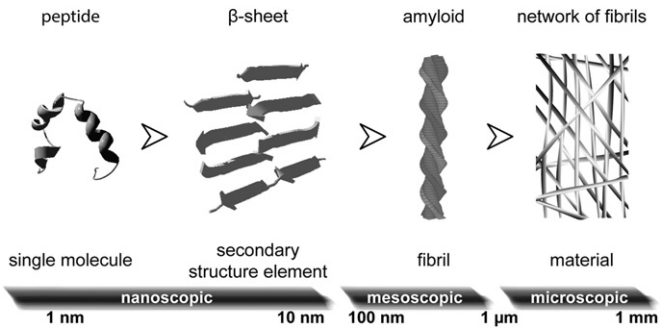

Fig. 1. Hierarchical length scales relevant in amyloid research, starting from the level of single molecules (*left side*: hIAPP, PDB 2L86) in the nanoscopic regime. Single or several peptides and proteins build up secondary structure elements, which are dominated in amyloids by β-sheets (PDB 2KIB). Mature amyloid fibrils have mesoscopic dimensions and consist typically of two or more twisted strands, forming thin and long fibrils. Networks of fibrils constitute micro- and macroscopic materials. Vibrational spectroscopies focus on insights at the molecule and secondary structure element level, atomic force and electron microscopy (AFM and EM) at the level of single fibrils and (micro-) rheology on networks of amyloids.

Specifically, this feature article describes recent investigations into the structural and mechanical properties of amyloids at different length scales. Nanoscopic level insights are obtained with recently developed vibrational spectroscopic techniques. The vibrations of molecular groups within amyloid structures, and in particular the amide I mode (with predominant C=O stretch character), are sensitive reporters of the local environment of those groups, as well as the protein structure. Hence, vibrational spectroscopies are very useful for quantifying secondary structure and intermolecular interactions in amyloid systems. Moreover, surface-specific vibrational spectroscopies like vibrational sum frequency generation (vSFG) can provide information about amyloid formation at (lipid-) interfaces, which are known to catalyze the polymerization of amyloid precursors. The application of tip-enhanced Raman spectroscopy (TERS) offers the possibility to spatially resolve structural characteristics of amyloids in the nm regime. Two-dimensional infrared spectroscopy (2D-IR) reveals amyloid interactions down to the level of single amino acids, by selective isotopic substitution.

At the mesoscopic level, we review results from biophysical assays using transmission electron-, atomic force and fluorescence microscopy to measure single fibril mechanical properties. Among others, several different approaches to determine values for bending rigidity, shear modulus, ultimate tensile strength and extensibility are presented. Rheology measurements have been applied at the microscopic scale to access the mechanical properties of networks of fibrils, which constitute promising materials like viscoelastic gels.

2. Background

Many biological materials rely on fibrous networks of proteins for their mechanical strength. Some well-known examples include tissues such as skin, blood clots, and spider webs. Proteins are normally folded in a specific geometry dictated by their primary structure (amino acid sequence). Fibrils are then formed by supramolecular assembly of protein building blocks, which are often globular (as in the case of actin and microtubules) or rod-like (as in the case of collagen and fibrin blood clots).

There is also an alternate path of fibril formation: misfolded or partially unfolded proteins tend to form amyloid fibrils. This pathway was originally discovered in the context of several neurodegenerative diseases (notably Alzheimer's, Parkinson's, Huntington's, and Prion disease) and late onset diabetes [13,14]. These 'conformational diseases' (or amyloidoses) are characterized by the deposition of insoluble plaques of aggregated amyloid fibrils, which can lead to cell death in specific organs. Surprisingly, several organisms use amyloids to build natural, protective materials, such as protective coatings of bacteria and spores and the silkmoth eggshell [15]. It is increasingly apparent that the amyloid state is an inherent characteristic of polypeptide molecules under denaturing conditions, independent of the native structure or primary sequence. In the context of food, this has been long known, for instance in the cases of heat-denatured gelation of β-lactoglobulin from milk and lysozyme from egg white [4].

Amyloid fibrils formed from structurally unrelated peptides and proteins share a surprisingly similar structure. The change in secondary structure of the native protein to a β-sheet rich secondary structure represents one of the main determinants of amyloid formation. Amyloid fibrils show a characteristic X-ray diffraction pattern, caused by a so-called cross-β core structure. The amyloid core structure is composed of a stack of β-strands perpendicular to

the fibril axis separated by 4.8 Å and with an intersheet spacing in the order of 9–11 Å [16,17]. The elongated stack is stabilized by a dense network of hydrogen bonds. The sequence-specific side-chains tend to affect the propensity to form fibrils [18]. A model of a protofibril from human amyloid polypeptide hIAPP is shown in Fig. 2. A single hIAPP molecule forms two β-sheets, separated by a loop region. The views along the entire fibril axis in the model reveal the dense stacking of four β-strands from two individual IAPP molecules per layer. This in-register packing of parallel β-sheets is one of the prominent characteristics of amyloids. A view perpendicular to the fibril axis (Fig. 2D) illustrates the 4.8 Å spacing between the stacks of parallel β-sheets and their parallel orientation to the fibril axis. Two or more protofibrils usually twist together to form unbranched, elongated mature amyloid fibrils which look like twisted rope-like structures or flat tapes, depending on the protein Ref. [12]. The high degree of structural order within fibrils leads to very strong interactions between the protofibrils within a mature amyloid fibril (for instance 310 $k_BT/\mu m$ for insulin Ref. [19]). The fibrils are typically about 10 nm in width (with a range of 5–25 nm) and up to 10 μm in length.

The unique molecular organization of amyloid fibrils endows them with remarkable mechanical properties. Amyloid fibrils are among the stiffest biological materials presently known, with a Young's modulus on the order of 3–20 GPa [4]. Moreover, amyloid fibrils exhibit a high resistance to breakage. Their ultimate strength was shown to be on the order of 0.6 GPa, comparable to the strength of silk but also steel [2]. This large fracture strength seems surprising since amyloid fibrils are held together by non-covalent interactions. Recent experimental and theoretical work has demonstrated that the remarkable rigidity of amyloid fibrils originates from the regular network of intermolecular hydrogen bonds in the cross-β core [3]. Non-covalent interactions between the variable side-chains (hydrophobic or hydrogen-bonding) sometimes further stabilize the fibril and enhance the Young's modulus [3].

From a materials science perspective, the amyloid pathway to form protein fibrils has many advantages. The fibrils readily self-

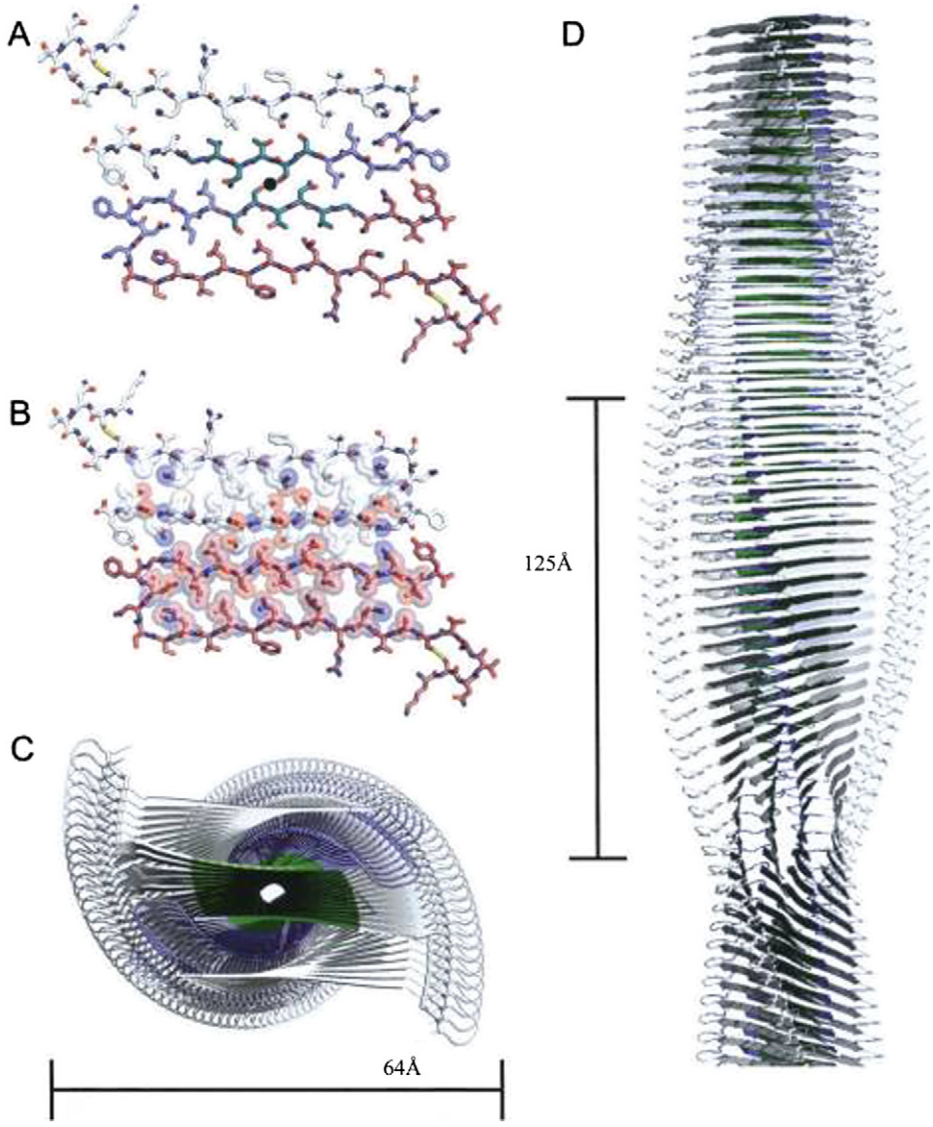

Fig. 2. Structural model of an amyloid protofibril from human islet amyloid polypeptide (hIAPP) based on the crystal structure from segments of the peptide. A–C View along the fibril axis. A. Two hIAPP molecules, each consisting of a hairpin and a steric zipper interface, tending to the fibrils axis. The space filling model B. emphasizes the tight steric zipper interface of the two IAPP molecules. C. Stacking of β-sheet segments which are coiled up around the fibril's axis. D. View perpendicular to the fibril axis, revealing the typical 4.8 Å spacing between layers of stacked β-sheets. The width of the fibril is 64 Å, the marked 125 Å distance matches a quarter of a full helical turn. Reprinted with permission from Ref. [17]. Copyright 2008 The Protein Society.

assemble from natural proteins including edible proteins (such as β-lactoglobulin) or pharmaceutically relevant proteins (such as insulin [19,20]), but they can also be formed from simple *de novo* designed peptides [21,22]. Fibrils can also be formed from proteins or peptides fused with functional proteins or peptides such as enzymes or cell adhesion motifs [9,23]. The mechanical properties are remarkably insensitive to the protein sequence [4], and robust under extreme conditions, such as high temperature, high concentrations of detergents and denaturants, as well as strong physical forces [6]. All of this makes them attractive candidates for applications. Indeed, there has recently been a surge of activity directed at designing materials from amyloids [7]. Amyloid fibrils have been coated with metal [6] and conducting polymers [24] to form conducting nanowires. Since amyloids are biocompatible, their use as drug delivery vehicles [8] or applications in tissue engineering [9] are also highly promising.

However, the flipside of the remarkable stability of amyloid aggregates is that such stability is undesirable during the production and storage of pharmaceutical and industrial peptides [25]. More importantly, the stability is also particularly undesirable in the context of conformational diseases, such as Alzheimer's and Parkinson's disease and type II diabetes, where amyloid fibrils are the cause of disease symptoms and accumulate in tissues because they cannot be degraded. More than 20 proteins that are partially unfolded, misfolded, or aggregated are known to give rise to amyloid fibrils in humans. There has been an intensive search for small molecules and peptides that can inhibit the formation of fibrils [14,26]. Originally, it was believed that the fibrils were the major toxic species (the 'amyloid hypothesis'). However, recently it has become apparent that oligomeric species may be even more toxic [27]. Thus, small molecule or peptide-based drugs should not only inhibit fibrillization, but also divert polypeptide assembly down alternative, less harmful assembly pathways [28].

Here we focus mainly (but not exclusively) on two exemplary amyloids, the disease-related human amyloid polypeptide (hIAPP) or amylin and the primarily food-related β-lactoglobulin (β-lg). hIAPP forms extracellular deposits in the pancreas of type 2 diabetes mellitus patients [29]. hIAPP is *in vivo* cosecreted with insulin by the β-islet cells of the pancreas. Amyloid fibrils and/or oligomeric forms of hIAPP are thought to induce cell death of islet cells, eventually destroying insulin production [29–32]. For *in vitro* studies, hIAPP is commonly prepared by solid-state synthesis, since it is a short peptide of 37 amino acid residues. In contrast, β-lg is a globular protein from milk that is of great interest for industrial (food) applications [33]. Amyloid fibrils can be readily formed by heat-induced denaturation at low pH [34–37]. Both hIAPP and β-lg are examples for well-studied systems in terms of kinetics and thermodynamics of formation (β-lg [36,38]; hIAPP [39]) and fibril structure (β-lg [34,37]; hIAPP [17,40–42]).

Recently, plant polyphenols have drawn attention as a possible candidate to control amyloid formation and stability. For instance, polyphenols are promising as a drug for prevention or treatment of Alzheimer's disease [4,43,44], and affect the quality of food-related materials [45]. They are ubiquitous compounds in plant-derived food and beverages (e.g. green tea) and have recently been shown to be potential inhibitors of amyloid fibrillization [43,44,46]. Polyphenols are thought to have many more beneficial properties based on their antimicrobial properties and their antioxidative capacities, including therapeutic potential for cancer [47] and cardiovascular diseases [48]. The strong interactions between polyphenols and amyloid proteins could potentially be used to combat amyloidosis, but proteins could also serve as delivery vehicles of polyphenols in the form of polyphenol-rich food or of drug delivery agents. Polyphenols are thought to interact with amyloids and amyloid precursor proteins via aromatic residues [49–51].

3. The nanoscopic level – spectroscopic insights into the molecular structure of amyloids

Vibrational spectroscopy is being widely applied for structural analysis of biopolymers. In this article, we will refrain from a description of classical Raman and FT-IR spectroscopy, despite the significant importance of these techniques in current amyloid research [52,53]. We will focus on "new techniques" with only a very brief and fragmentary description of the techniques themselves, rather emphasizing the new insights into amyloid fibrils provided by such techniques with the use of a few significant examples.

The development of two relatively new vibrational techniques, coherent two-dimensional infrared spectroscopy (2DIR) and vibrational sum frequency generation spectroscopy (vSFG) have depended strongly on the development and common availability of infrared laser systems with ultra-short pulse duration. Their application to biopolymers is still at its beginning, not only providing the general structural sensitivity of vibrational spectroscopy but further offering an intrinsic possibility to perform ultrafast time-resolved experiments down to femtoseconds, the time domain of formation and breaking of chemical bonds [54]. Tip-enhanced Raman scattering (TERS) provides another route towards the investigation of nanoscale structural variations, utilizing plasmonic particles for sensitivity enhancement and spatial resolution improvement [55,56]. TERS enables even the investigation of the polymorphism of single amyloid fibrils [57]. In the following, recent results obtained with these three vibrational spectroscopic approaches are highlighted.

3.1. Vibrational sum frequency generation spectroscopy (vSFG)

Vibrational sum frequency generation spectroscopy (vSFG) emerged after the development of ultrafast infrared lasers as a technique mostly applied under ultra-high vacuum (UHV) conditions to characterize the vibrational spectra of molecules adsorbed onto surfaces. Nowadays vSFG is routinely applied to complex biologically relevant samples, with its rather unique surface specificity, combined with high sensitivity and time resolution [54,58,59]. The main strength of vSFG is that it allows one to record the vibrational spectrum of specifically the outermost monolayer of a bulk material, with high sensitivity.

In a typical vSFG experiment, ultrashort amplified laser light pulses (e.g. at a wavelength of 800 nm) are split to allow for the subsequent generation of spectrally narrow visible and broadband mid-infrared laser pulses. The two coherent pulses are spatially and temporally overlapped onto the sample surface and interact with the interface by generating light of the sum frequency of the visible and mid-infrared light. This process is enhanced if the infrared light is in resonance with vibrational modes on the surface. Using spectrally resolved detection, the frequencies of surface vibrations are readily extracted from the vSFG spectra by subtracting the frequency of the narrowband visible pulse. The resulting vSFG spectrum is usually normalized to the non-resonant vSFG signal of a reference material or the intensity spectrum of the broadband IR laser pulse (for a detailed review we refer to [54]). Heterodyne detection may be applied to obtain not only intensity, but also amplitude and phase information of the spectra, an approach which is helpful in particular if vibrational modes strongly overlap.

In addition to its sensitivity, the specificity of vSFG to non-isotropic samples offers the remarkable possibility to measure structurally sensitive vibrational spectra exclusively at interfaces. Isotropic bulk media show no SFG spectra due to the selection rules of the underlying second-order nonlinear optical process. The second-order polarizability, the source term of the SFG light, is zero

for any medium with inversion symmetry. At interfaces, the symmetry of the centrosymmetric bulk phase is broken, allowing for measurements of vibrational spectra specifically at the interface.

The sensitivity of vSFG to surface monolayers enables for instance the investigation of the very same amyloid samples which are suitable for atomic force microscopy (AFM) as well. Therefore a molecular method can be directly aligned to a mesoscopic method. This approach can be applied to consecutively analyze secondary structure and e.g. stiffness parameters of amyloids grown at different conditions. The spatial resolution of a typical SFG setup is restricted by the size of the two overlapping laser pulses. Typically, the SFG signal is averaged over an area somewhat less than one square millimeter. The application of AFM and SFG together allows therefore the combination of a high spatial resolution technique with a surface sensitive label-free vibrational spectroscopy.

The combination of vSFG and tapping mode AFM was used to characterize different morphology forms of amyloids grown from β-lactoglobulin [60]. It was shown that β-lg forms small, worm-like amyloids when grown under high concentration (7.5% w/v) conditions and long, straight fibrils at lower protein concentration (3% w/v) [60]. The stiffness of the two morphologically different amyloid forms differs strongly (see below), even though they display the same fibril diameter. vSFG was applied to reveal the molecular origin of this surprising behavior [60]. In Fig. 3a, vSFG spectra in the amide I spectral region of amyloid fibrils obtained from different growth conditions are presented. The position of the vSFG band enables the determination of the secondary structure distribution of the samples. Fig. 3b depicts the resulting secondary structure analysis along with two representative AFM images of the amyloid fibrils. It could be shown, that the small, worm-like amyloids of β-lg grown under high concentration (7.5% w/v) conditions, exhibit a high content of α-helical/unordered structures. For the long fibrils, formed at lower protein concentration (3% w/v), a strong content of β-sheets could be detected. The fibril persistence length (or bending rigidity) apparently decreases for an increasing content of α-helical/unordered secondary structure. Whereas for straight fibrils with a strong β-sheet content a persistence length of 3820 ± 160 nm was found, the worm-like fibrils had a persistence length of only 92 ± 7 nm [60]. While the influence of secondary structure on the stiffness of amyloid fibrils could be unambiguously demonstrated, the precise spatial distribution of secondary structure remains unclear. Structure sensitive methods with inherent high spatial resolution like tip enhanced Raman scattering (TERS, see also below) may in the future address the question how fibrils can be built up with such remarkable differences in their secondary structure composition, and yet be of the same thickness.

In vivo, the growth of amyloid fibrils, as well as the cytotoxic effect of fibrils or their oligomeric precursors, is thought to take place on the plasma membrane of cells [30,31]. The possibility of vSFG to exclusively detect signals from model membranes like the air–water interface of lipid monolayers provides the opportunity to measure structural properties of amyloid fibrils under more biologically relevant conditions than with conventional vibrational spectroscopy techniques. In their pioneering work on amyloids forming at lipid monolayer interfaces the Yan group employed surface-selective SFG to monitor structural changes of islet amyloid polypeptide during fibrillation [61,62]. Subsequent they reported on the orientation of human IAPP amyloids, based on polarization dependent SFG studies in combination with *ab initio* calculations [63]. hIAPP is involved in the death of insulin producing islet cells of Langerhans [29]. With SFG, the misfolding of hIAPP from an α-helical or unordered form to a β-sheet rich amyloid structure was kinetically resolved under the catalyzing action of negatively charged phospholipids [61].

As mentioned in the background section, polyphenols like (−)-epigallocatechin gallate (EGCG) are promising inhibitors of amyloid formation in the context of various amyloid-related diseases. Applying the experimental conditions employed by the Yan group [61], we tested the inhibitory action of EGCG using the surface specificity of SFG at the phospholipid interface. Fig. 4 summarizes the experiments following the changes in secondary structure of human IAPP in the amide I spectral region. Without inhibitor, a structural transition from an α-helical or unordered secondary structure to a β-sheet rich structure was observed by a shift of the amide I band from 1652 cm^{-1}–1672 cm^{-1} [64]. This secondary structure transition was interpreted as the formation of amyloid fibrils (see Fig. 4a), as verified by AFM measurements on the same samples transferred to a solid substrate. In the presence of the inhibitor EGCG the structural transition is less pronounced, but still obvious [64]. This observation is in strong contrast with the situation in bulk. A standard biophysical technique for detecting amyloids in solution is the Thioflavin T (ThT) fluorescence assay. Upon binding of Thioflavin T to β-sheet rich amyloids, an enhanced and red-shifted fluorescence is observed, as shown in Fig. 4c for the

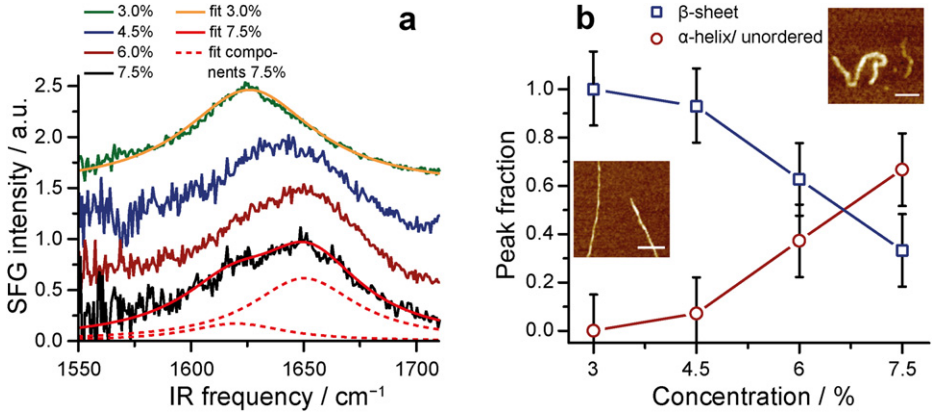

Fig. 3. a. SFG spectra of β-lactoglobulin amyloids on mica in the amide I spectral region. Amyloid fibrils were grown for different monomer concentrations, as indicated in % w/v. The spectra allow for a secondary structure analysis of the samples by fitting the vibrational SFG band with two components, corresponding to the contribution of α-helices or unordered structures (around 1652 cm^{-1}) and β-sheets (around 1629 cm^{-1}). b. Quantitative analysis of the SFG spectra shows, that amyloid fibrils grown under higher concentration conditions (6 and 7.5% w/v) exhibit higher α-helical or unordered structural content, and a less pronounced β-sheet structural content. AFM imaging of the β-lactoglobulin amyloid samples on mica shows a morphology change from long, straight fibrils at low concentration to worm-like ones at higher concentrations (the white bar corresponds to a length of 100 nm). This transition is evidently accompanied by a change in secondary structure. Figures are based with permission on [60]. Copyright 2011 American Chemical Society (Minor corrections of the peak fractions in b. were performed, which do not affect the general trend of the original figure).

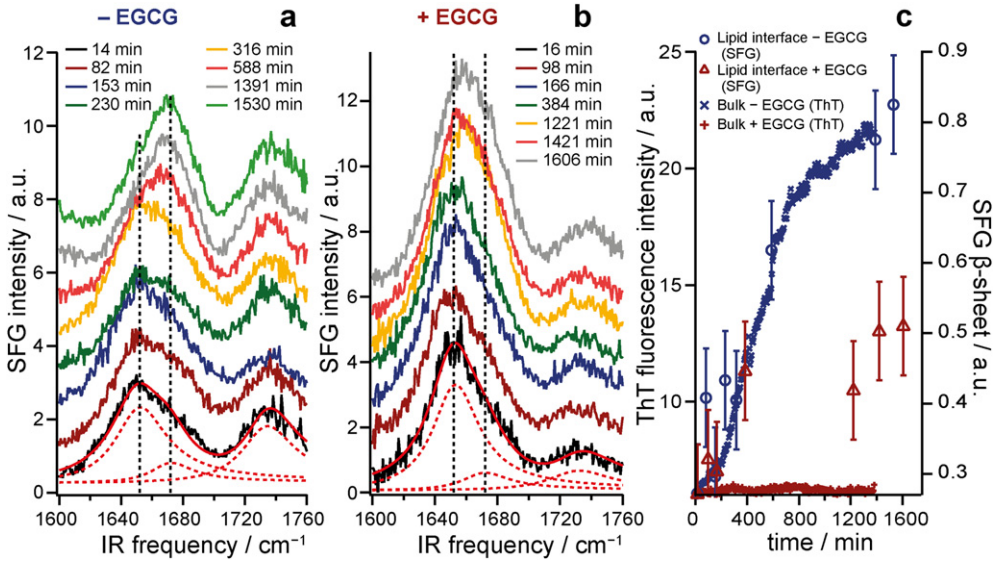

Fig. 4. a. Fibrillation of human islet amyloid polypeptide (hIAPP) followed by SFG at a phospholipid monolayer-covered water/air interface. At early times, the amide I band is centered at 1652 cm^{-1}, corresponding to a mainly α-helical or unordered secondary structure. For later times a shift of the amide I band to 1672 cm^{-1} is observed, denoting a β-sheet rich structure, characteristic for amyloids. b. hIAPP fibrillation followed in the presence of the inhibitor EGCG. The formation of β-sheets is less pronounced, but still evident. Fitting of three bands (as exemplified for the earliest time by the broken red lines in a and b) to the SFG data allows a quantification of the β-sheet contribution to the spectrum. c. A comparison of the β-sheet spectral contribution, revealed by SFG for the lipid interface situation and the fluorescence intensity of a Thioflavin T assay for bulk solutions. Both situations are plotted in the absence (blue ○ for SFG and blue × for ThT assay) as well as in the presence of the inhibitor EGCG (red Δ for SFG and red + for ThT assay). The effect of the inhibitor EGCG is strongly diminished at the interface, compared to the bulk situation. Adapted with permission from Ref. [64]. Copyright 2012 American Chemical Society.

formation of IAPP amyloid fibrils in bulk solution (see trace marked by blue ×). In the presence of the inhibitor EGCG, no increase in fluorescence could be detected (red +). The combined experiments at the interface and in bulk solution lead to the conclusion, that whereas EGCG is a potent inhibitor in bulk, its inhibitive effect at the membrane interface is strongly reduced. The membrane interface represents the biologically relevant location of the cytotoxicity of hIAPP. Even more pronounced is the difference between bulk and lipid interface for the disaggregation of pre-formed amyloids by EGCG. The ability of EGCG to dissolve preformed aggregates in bulk solution could be verified again by a ThT assay as depicted in Fig. 5a (blue ×). The fluorescence rapidly decreases after addition of the inhibitor, indicating a fast disaggregation. SFG is able to monitor the effect of EGCG exclusively at the lipid interface (red Δ). Even after incubation times up to 30 h (Fig. 5a) or after addition of a 1000-fold molar excess of EGCG compared to the hIAPP concentration (Fig. 5b), the β-sheet content of the sample stays constant. AFM confirmed the presence of fibrils after treatment with EGCG (see inset in Fig. 5b). In conclusion, at the lipid interface the inhibitor EGCG is not able to dissolve amyloid fibrils at all. The molecular origin of these findings is the subject of ongoing research, but the results clearly highlight the importance of structural information gained selectively at interfaces.

vSFG offers many possibilities for future studies that can address more complex, biologically relevant problems. For instance, the inherent fast time-resolution of vSFG may be exploited to reveal short lived oligomeric states during amyloid formation or disaggregation. While applications of whole cells in pharmaceutical studies of amyloids are well documented [46,65], recently vSFG was applied on fibrillar proteins of the extracellular matrix of living cells as well. In future experiments, the complexity of *in vivo* tests is therefore not beyond the means of vSFG [66].

3.2. Tip-enhanced Raman scattering (TERS)

A combination of the excellent spatial resolution of AFM and the structural sensitivity of vibrational spectroscopy in a single setup is realized by tip enhanced Raman spectroscopy (TERS). TERS is becoming an increasingly off-the-shelve tool for label-free structural investigations of nanoscale phenomena at surfaces. Recent results have demonstrated a lateral resolution down to the sub-

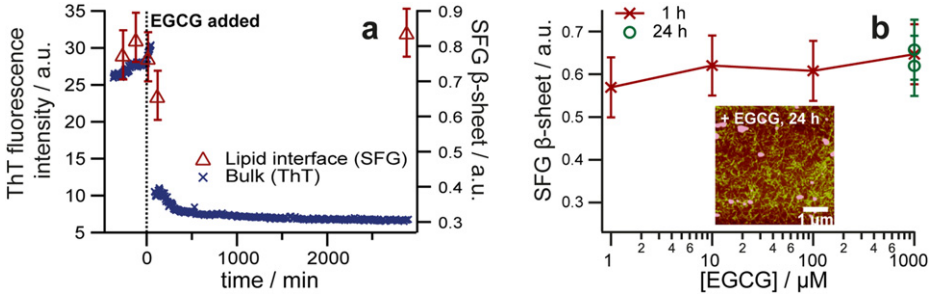

Fig. 5. a. Disaggregation of preformed hIAPP fibrils, followed by the amount of β-sheet secondary structure using SFG at the phospholipid interface (red Δ) and the fluorescence intensity of a ThT assay in bulk solution (blue ×). At time zero, EGCG is added, which leads to a rapid fibril disaggregation in bulk, whereas no disaggregation takes place at the lipid interface. b. Even a 1000 fold molar excess (1000 μM) EGCG does not lead to a significant decrease in the β-sheet content. The presence of fibrils is verified by AFM imaging (see inset). Based on [64] with permission. Copyright 2012 American Chemical Society.

nanometer range. Clearly, this renders the method a valuable tool for the direct investigation of single polymer strands.

One of the key components of a TERS setup is a plasmonic tip, like a sharp edge of gold or an isolated gold or silver nanoparticle. The external, monochromatic electromagnetic laser field oscillates at a given frequency, which drives the electrons in the plasmonic structure to perform a periodic motion. The resulting oscillating dipole may increase the strength of the electromagnetic field in the immediate vicinity of the plasmonic structure by many orders of magnitude. Raman scattering can take place in molecules under the plasmonic structure. Because both the incident and scattered Raman fields are amplified by the plasmonic effect, the Raman field scales linearly with the incident field, and because the detected Raman intensity scales with square of the Raman field, the Raman intensity enhancement scales with the fourth power of the local field enhancement. As a result, extremely low concentrations down to single molecules can be investigated. The size of the nanoparticles determines the spatial extent of the field-enhancing region and as a rule of thumb the lateral resolution in TERS is about half of the radius of the nanoparticle. In addition further enhancement mechanisms due to interactions between the metal particle and the investigated molecule can occur (so called chemical enhancement). Interestingly the depth resolution is even higher than the lateral resolution. According to simulations the electromagnetic field decays very fast and the z-resolution is in the range of 1–2 nm. Also here, a direct interaction also increases this depth resolution.

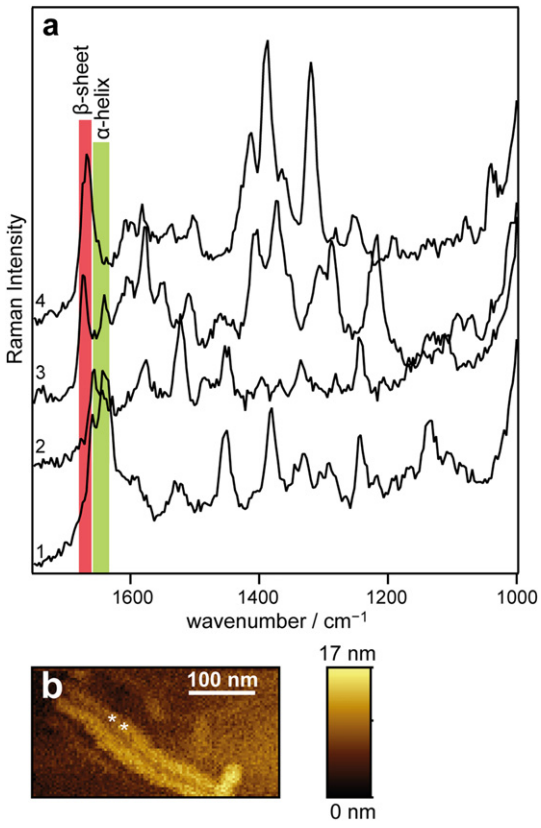

Fig. 6. a. Four raw TERS spectra obtained from a single IAPP fibril (generated at pH 7). Spectra 1 and 2 were recorded at a relative lateral distance of 1.5 nm at the position marked by the upper * in panel b. and show characteristic bands of α-helix secondary structures (highlighted in green). Spectra 3 and 4 were recorded at a relative lateral distance of 1.5 nm at the position marked by the lower * in panel b. and show in contrast characteristic bands of β-sheet structures (highlighted in red). b. Typical AFM topography of IAPP fibrils (generated at pH 7). TERS spectra were acquired on the top fibril at two areas (marked with *), each with two positions separated by 1.5 nm, respectively.

These properties are ideally suited to investigate amyloids with a thickness of a few nm and length in the micrometer scale. The correlation of a topographic image of a fibril with the spectral map could possibly reveal the surface structure of complete fibrils. The polymorphism of single amyloid fibrils gets therefore directly accessible.

An inherent characteristic of TERS is the ability to analyze the topographic and chemical structure of a specimen in one experiment. Fig. 6 shows the results of such an experiment on a single segregated hIAPP fibril. In Fig. 6a selected TERS spectra show the typical Raman signals of a protein. The detection sites on the fibril are marked in the topography image in Fig. 6b.

The spectral range in Raman spectroscopy that gives information on the secondary structure of a specimen is the amide I region between 1640 and 1680 cm^{-1}. The bands highlighted in red (1660–1680 cm^{-1}) in Fig. 6a are characteristic for β-sheet structures whereas the bands highlighted in green between 1640 and 1655 cm^{-1} are marker bands for α-helix structures. The detection of both conformations on hIAPP fibrils indicates that the surface is composed of a heterogenous secondary structure. This is different from the core structure, which is known to be pure β-sheet. Such observations have been made previously on insulin [67] fibrils and give rise to the assumption that such heterogeneity is a common feature of amyloid fibrils. The role of such conformation mixtures is still under investigation.

The diversity of the spectra in Fig. 6a recorded on positions at nanometers distance, demonstrates the ability of TERS to differentiate protein structures on the nanometer scale. Besides a characterization of secondary structures on fibrils this specialized Raman spectroscopic technique provides information about the amino acid distribution on the fibril, also with nanometer resolution [57]. It is evident that this approach can be of great assistance for understanding the fibrillation process trigger and/or mechanism on the nanometer scale.

In addition to having the ability to address amyloid fibril polymorphism, TERS holds the possibility to elucidate the role of single amino acids in determining fibril stability and mechanical properties. This is an important issue, as the side chains of amino acids have been shown to contribute to the stability of the β-cross core of amyloids, affecting the elastic modulus of fibrils [3].

3.3. Coherent two-dimensional infrared spectroscopy (2DIR)

2DIR has become a powerful tool for the structural investigation of proteins. By addressing localized vibrational transitions using a specific sequence of infrared laser pulses, details of the molecular response can be obtained, which can be related to structure and structural evolution. The structural information contained in respective linear spectra is essentially mapped onto two dimensions. The essence of 2DIR spectroscopy is that one specific vibrational mode is selectively excited, and the effect of that excitation is monitored on both that same mode, and on other vibrational modes. From the study of the mode itself, the distribution of vibrational frequencies can be obtained, as well as the timescale on which these frequencies change, as a result of conformational fluctuations, for instance. If the excitation has an effect on a different mode, this means that the two molecular groups primarily responsible for the modes are physically close to one another. The strength and nature of the resulting coupling can be related to the local structure, and structural rearrangement (basic details can be obtained from the textbook [68]).

2DIR spectra can be recorded either in the frequency domain or in the time domain, which both results in basically identical spectra

[69]. Experiments in the frequency domain are realized by the pump-probe technique. A scanning, spectrally narrow IR pump pulse excites vibrational transitions and a spectrally broad probe pulse identifies the exited vibrations after a fixed time from the pump pulse. The 2D spectrum is constructed by plotting the measured probe spectra for each applied pump frequency.

For 2DIR experiments in the time domain, also named echo spectroscopy, three sequential IR pulses are applied to generate the echo signal. The latter is recorded with a varying delay between the two first (pump) pulses and a fixed delay between the second pump and last (probe) pulses. Heterodyne detection is applied to extract both amplitude and phase information. The construction of a 2D spectrum involves a Fourier transformation: if the probe spectra are plotted against a full set of the time delays between the two pump pulses, a damped oscillation in the recorded intensity for each probe frequency is yielded. This is analogous to multidimensional FT-NMR correlation spectroscopy, where a free induction decay (FID) is measured for a sequence of radio frequency pulses. By means of Fourier transformation of the time-domain signal a pump spectrum in the frequency domain is obtained for each measured probe frequency.

A typical 2DIR spectrum contains valuable information, additionally to linear spectroscopy. Diagonal elements refer to peaks near the diagonal of the 2D spectrum. They originate from excited vibrational states, leading to higher order absorption (e.g. from the first to the second excited state), resulting in positive peaks and emission processes resulting in negative bands slightly shifted with respect to the positive ones. Due to fast vibrational relaxation processes occurring between pump and probe pulses, additional negative bands may arise due to absorption of the probe beam from vibrational ground states. The main characteristics of 2DIR spectroscopy are the cross-peaks, which arise from coupled vibrational modes. Knowledge on vibrational coupling in terms of distance and angular dependence can be transferred to structural information. In complex systems like biomolecules often models based on molecular dynamics simulations are implemented to extract structural information from vibrational coupling [70]. 2D band shapes include additional structural information and are influenced by environment effects such as hydrogen bonding or solvent effects [71].

Additionally to the structural sensitivity of 2DIR, transient 2DIR permits probing of the kinetics of structural transitions with subpicosecond time resolution, for instance in case of chemical reactions [72,73].

A widely used application of 2DIR is the secondary structure analysis of proteins. 2DIR is regarded as being more accurate than 1D FT-IR because of the increased information content achieved by having information on both excitation and detection axes, and the above-mentioned high time-resolution [74,75]. Isotopic labeling of specific amino acids can be employed to reveal the site-specific, local secondary structure of proteins [71]. Additionally, challenges like heterogeneity within a protein, protein–protein interactions or ligand binding can be addressed [70]. Although secondary structure analysis is quite accessible with 2DIR, investigations of the tertiary structure of proteins are performed in combination with molecular dynamics calculations to distinguish between different tertiary structure types. A practical drawback of the technique is the requirement of high sample concentrations, when compared to traditional 1D FT-IR or monolayer sensitive vSFG.

A recent example of a detailed structural analysis of amyloids from hIAPP was reported by Wang et al. [73]. The authors combined experimental information from 2DIR spectroscopy with calculations of 2DIR spectra and MD simulations of hIAPP, allowing for conclusions on the structure of hIAPP fibrils beyond secondary structure analysis. Based on the fact that the diagonal line widths of the amide I peak of single amino acids differ for residues from a β-sheet and C-terminal or turn-structures, the authors deduced the number of folds of β-structures within the peptide. Experimentally, they employed seven samples with (diluted) site-specific $^{13}C{=}^{18}O$ labeled amino acids. It was therefore possible to test the secondary structure of hIAPP specifically on seven distinct locations along the peptide chain. The diagonal amide I peaks of the labeled amino acids showed a pronounced down shift compared to the unlabeled amino acids and could be investigated mostly undisturbed by the unlabeled part of the protein. Plotting the line widths of labeled amide I peaks against the residue number, Wang et al. observed a characteristic "W-shape" pattern. This pattern was assigned to the presence of two stable β-sheet regions connected by a turn-structure within a single amyloid-forming hIAPP monomer. The pattern could be compared to calculated 2DIR spectra based on previously proposed structural models of hIAPP amyloids relying on solid state NMR and electron microscopy studies [76,77].

The Zanni group, involved as well in the above mentioned study, reported on the residue-specific kinetics of hIAPP aggregation [78], employing isotopic labeled amino acids on six different positions within the peptide. Based on the time-resolved site-specific formation of β-sheets it was possible to conclude on requirements for a model of the hIAPP aggregation pathway. Such a pathway was found to be more complex than a simple pathway requiring a random-coil intermediate, which undergoes a concerted transition to a fiber-like nucleus and subsequent elongation by the addition of monomers [78].

2DIR contributed further to the elucidation of structural transitions during the formation of amyloids [78–80], as well as the effect of inhibitors on amyloid formation [81]. Meng et al. reported on the effect of an inhibitor based on a sulfated triphenyl methane derivate on the formation of amyloids from hIAPP. 2DIR revealed an influence of the inhibitor on the β-sheet content of the samples, as shown in Fig. 7. In Fig. 7a, the 2DIR spectrum of the pure hIAPP fibrils shows two diagonal out-of-phase features (doublets). A strong one at the pump frequency of 1619 cm^{-1}, corresponding to a predominant β-sheet secondary structure [71], as well as a weaker, broad feature at 1646 cm^{-1}, consistent with an unordered structure [81]. In the presence of inhibitor, a strong decrease in the peak intensities attributed to the β-sheet structure is evident (Fig. 7b). A smaller effect is an accompanying frequency shift of 3 cm^{-1} to higher frequencies compared with pure hIAPP samples, which the authors attributed to a smaller size of the β-sheets.

The interaction of a peptide-based inhibitor of hIAPP fibril formation was investigated by Middleton et al. [28]. The authors applied isotopic labeling for a residue-specific 2DIR analysis of the inhibitory effect of rat IAPP (rIAPP) on hIAPP fibrillation. For this purpose, they incubated the inhibitor and the amyloid peptide for a short (8 h) and a long time (24 h) after mixing. rIAPP was known not to form fibrils under any conditions, but represents a moderate inhibitor of hIAPP fibril formation (for *in vitro* tests a strong inhibition of fibril growth requires approximately a tenfold molar excess of rIAPP [82]). A first finding was the identification of the inhibitor binding side by the fact that the N-terminal β-sheet of hIAPP is not formed within 8 h in the presence of rIAPP (Fig. 8a). This result explained the structural basis of the slower amyloid formation in the presence of the inhibitor. After long-time incubation of inhibitor and hIAPP, fibril formation was not inhibited. Surprisingly it was found, that rIAPP and hIAPP form mixed amyloidogenic parallel β-sheets 24 h after mixing (Fig. 8b). The structural sensitive 2DIR technique could reveal therefore a potential additional toxicity of an agent, which was previously thought to combat amyloid formation. Structure sensitive 2DIR proved therefore as a very fruitful technique for the investigation of amyloid formation and inhibitor interaction, in particular because

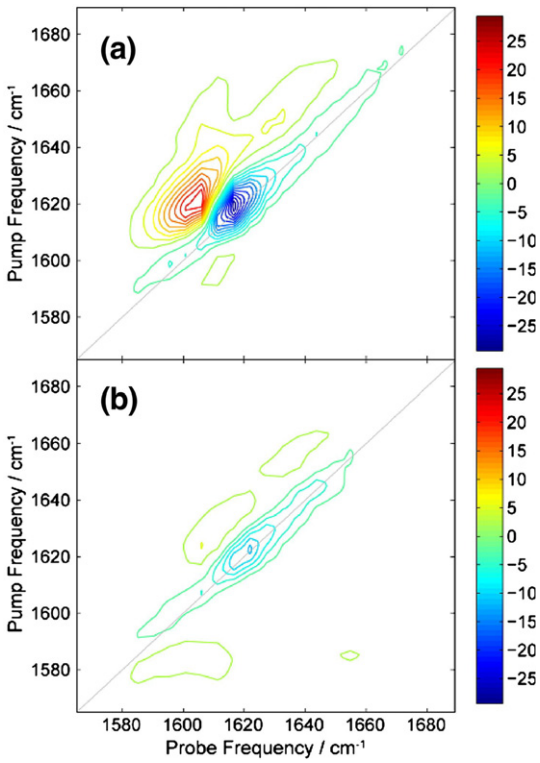

Fig. 7. 2DIR spectra in the amide I spectral region of hIAPP after formation of amyloids in the (a) absence or (b) presence of an inhibitor based on a sulfonated triphenylmethyl derivate. The same growth conditions were applied. Reprinted with permission from Ref. [81].

standard fluorescence techniques (Thioflavin T assay) suggested that the system already equilibrated after 8 h [28], contrary to 2DIR.

More complex experiments like 3DIR approaches or additional pulse sequences [68] may in future further strengthen the application of multidimensional IR correlation spectroscopy to structural characterization of biopolymers.

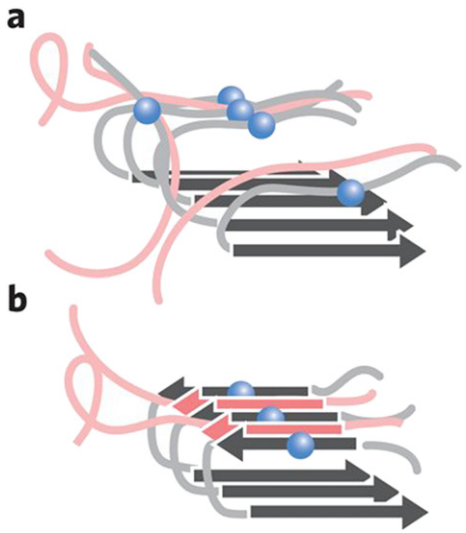

Fig. 8. Model structures of the co-aggregated hIAPP (grey) and rIAPP (pink) a. 8 h and b. 24 h after mixing of the peptides. One site-specific isotopic labeling side of hIAPP is depicted as blue spheres. In a., rIAPP prevents initially the N-terminal formation of β-sheets of hIAPP. In b., mixed β-sheets from hIAPP and rIAPP are formed. Reused with permission from Ref. [28]. Copyright 2012 Macmillan Publishers.

4. Mesoscopic properties of single amyloid fibrils

Proteins and peptides form amyloid fibrils by self-assembling into protofibrils, which have a β-sheet core. Usually, between 2 and 4 protofibrils subsequently twist together to form a mature fibril [83–85]. Amyloid fibrils tend to be highly polymorphic, varying in length and in the number of protofibrils. The β-sheet core makes amyloid fibrils rigid with a Young's modulus similar to that of silk and strong with an ultimate tensile strength comparable to that of steel [2]. Because of their outstanding mechanical properties, amyloid fibrils are promising structures for applications in biomaterials and food technology. However, the mechanical properties of amyloids are still not fully understood. There are several theoretical models which assign the large rigidity and strength of amyloid fibrils to their β-sheet core [3,86]. However, amyloid fibrils are polymorphic, and vibrational spectroscopy data indicate that the β-sheet content can be much less than 100%, as shown in Fig. 3. At least in part, this is a consequence of the presence of side-chains, whose effect on the mechanical properties of fibrils is unclear. In addition, amyloid fibrils may have imperfect β-sheet cores with interruptions along the long axis. Here we will review recent biophysical studies of the mechanical properties of single fibrils, and indicate some promising techniques that can be used in future to better understand the mechanics of amyloid fibrils and their origin.

4.1. Bending rigidity and shear modulus

A key parameter characterizing the conformation of a biopolymer is the bending rigidity. The bending rigidity is often expressed by the length scale beyond which the fibril shows significant curvature due to thermal forces, quantified by the persistence length P [87,88]. The bending rigidity can be measured by a variety of methods, which are either based on active deformation of the fibrils, or on analysis of the spontaneous, thermal bending fluctuations of the fibrils.

Active deformation of fibrils can be achieved by AFM, as demonstrated in a recent study on insulin amyloid fibrils composed of two protofibrils [2,3]. Essentially, the experiment was a microscopic equivalent of a traditional three-point bending test: fibrils were deposited on a silicon substrate with nanoscale grooves. With an AFM probe, a controlled load was applied on fibrils suspended over a groove, while monitoring the deflection of the cantilever that acts as the force sensor. The Young's modulus was determined from the linear (small-force) part of the deflection curve, giving an average Young's modulus of $E = 3.3 \pm 0.4$ GPa and shear modulus of $G = 0.28 \pm 0.2$ GPa. This Young's modulus corresponds to a persistence length of 42 ± 30 μm, which is much larger than the typical fibril contour length of 3–6 μm. An advantage of this technique is that the measurements are performed on fibrils in their natural, hydrated state. However, it is only possible to measure on the length scale of the tip radius, which is small compared to the fibrils. Also, the experiment is technically very challenging because of the small diameter of the amyloid fibrils [83].

Technically, it is far easier to measure the bending rigidity based on the spontaneous, thermal fluctuations of fibrils. The basic idea is to measure the shape of fluctuating fibrils, either taking snapshots of a large ensemble of fibrils at a given moment in time, or taking time-lapse movies of a single fibril. Until now, most studies of amyloid fibrils used the first method, analyzing the shape of a large ensemble of fibrils immobilized on a surface. Usually, amyloid fibrils are imaged by AFM [60,89–91], which requires fibril deposition on a mica or glass surface and drying. Alternatively, cryo-transmission electron microscopy (cryo-TEM) can be used, which has the benefit that fibrils are preserved (snap-frozen) in a hydrated state [92]. The persistence length P can be calculated by measuring

for each fibril the contour length, C, and the end-to-end distance, E (Fig. 9). According to the worm-like chain model, the mean-squared end-to-end distance on a two-dimensional surface as a function of C depends on P as in the following equation:

$$\langle E^2 \rangle_{2D} = 4PC\left(1 - 2P/C\left(1 - e^{-C/2P}\right)\right).$$

This equation assumes that the fibrils interact weakly with the surface and can relax to a two-dimensional equilibrium conformation [87,89,91]. However, if the interaction between the fibril and the surface is much stronger than the thermal energy, the fibrils will be trapped by the surface, leading to more condensed fibril conformations. In this case, the mean-squared end-to-end distance of the fibril amounts to [89]:

$$\langle E^2 \rangle_{3D} = 4/3PC\left(1 - P/C\left(1 - e^{-C/P}\right)\right).$$

An alternative method of determining P is by analyzing the correlation of bond angles along the contour:

$$P = \langle l \rangle / (1 - \langle \cos \varphi \rangle),$$

where $<l>$ is the average segment length and φ is the angle between segments (Fig. 9) [93].

One of the best-studied types of amyloid fibrils are those formed from the model protein β-lactoglobulin (β-lg). Depending on the self-assembly conditions, these fibrils have widely varying persistence lengths and mostly fall into one of two classes: straight fibrils or worm-like fibrils (Fig. 10a, b and Fig. 3b). Straight fibrils generally have a persistence length that is comparable to the contour length, ranging from about 600 nm to several μm [37,60,90,91,93–96]. Worm-like fibrils are much more flexible, with a persistence length of only 10–90 nm (Table 1) [37,60,89,91,93,94,96]. A third type of morphology, rod-like fibrils with a persistence length of 135 nm, was formed from β-2-microglobulin (Fig. 10c) [91]. It has to be noted that amyloid fibrils are polymorphic; even under a given set of conditions, fibrils have different persistence lengths. The numbers given in Table 1 are average values.

In contrast to nanomechanical manipulation assays, the fluctuation analysis approach gives a global measure of the persistence length of a fibril, because fluctuations are evaluated on a larger length scale. However, fibril imaging by AFM requires deposition on a surface and drying, which can potentially lead to artifacts.

One way to overcome this problem is to measure the shape of freely fluctuating fibrils in solution by fluorescence microscopy (Fig. 10d) [97,98]. Because of the low resolution of optical microscopes in the z-direction, fibrils are typically confined in a quasi-2D geometry by sandwiching them between two glass cover slips. Rather than extracting the persistence length from the static shape of an ensemble of fibrils, the persistence length is now calculated by tracking the fibril shape fluctuations over time. These experiments have been performed for yeast prion fibrils labeled with a fluorescent dye [98]. The persistence length was found to be 3.6 ± 1.1 or 7.0 ± 2.4 μm, depending on the assembly conditions. In addition to the bending rigidity, also the bending dynamics can be determined from time-lapse movies, as demonstrated for actin filaments and microtubules [88].

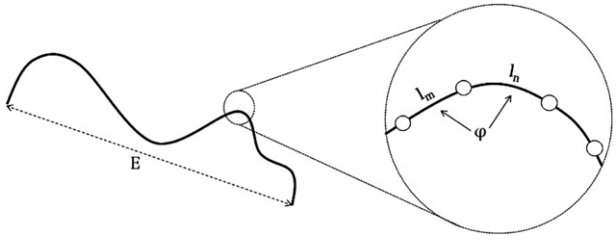

Fig. 9. Schematic depiction of the end-to-end length E, the segment length l, and the angle between segments φ, for a general semiflexible filament.

A second way to overcome problems associated with drying or surface immobilization is to perform light scattering of dilute fibril suspensions, again using the worm-like chain model to interpret the data. The persistence length of β-lg amyloid fibrils formed at varying ionic strengths was determined by a combination of light scattering (LS) and small-angle neutron scattering (SANS) [94]. The persistence length decreased with increasing ionic strength from 600 to 38 nm. These values are in reasonable agreement with the persistence lengths obtained with imaging techniques (Table 1).

The persistence length of β-lg fibrils also has been estimated using an adjusted random contact model, based on measurements of the storage (or elastic) modulus G' of fibril gels by rheology [37]. The critical percolation concentration was determined by measuring G' as a function of protein concentration. It was assumed that for a fibrillar system the percolation mass fraction is described by the volume of the fibril, the number of contacts per rod and the excluded volume of charged semiflexible fibrils. The volume of the fibril can be determined by the effective diameter, contour length and persistence length. The estimated persistence length was 1.6 ± 0.4 μm for β-lg fibrils formed at pH = 2 and 80 °C (Table 1, 7th entry).

4.2. Ultimate tensile strength and fracture behavior

The ultimate strength of single fibrils has been measured by nanomechanical manipulation with AFM. For insulin fibrils, the ultimate strength was measured by actively bending fibrils suspended over a groove with an AFM tip. The mean ultimate strength for fibrils composed of two protofibrils was 0.6 ± 0.4 GPa. Strikingly, this is in the same order of magnitude as the strength of steel (0.6–1.8 GPa) and silk (1.0–1.5 GPa) [2,3]. The corresponding breakage force was estimated to be in the range of 300–500 pN [2].

Microscopic insight into the molecular mechanisms that determine the strength of amyloid fibrils can be obtained by force spectroscopy, where peptide strands are pulled from fibrils immobilized on a surface with a small AFM tip. Such experiments were reported for fibrils formed from Aβ(1–40) or Aβ(25–35) peptides [99]. Strands of more than 100 nm in length could be pulled out of the fibrils and stretched. The force-extension behavior that was observed was fitted with a worm-like chain model, from which a persistence length of about 0.4 nm was calculated. Based on these results, the authors concluded that the strands were β-sheets that were unzipped from the fibrils. The unzipping process was fully reversible. Fibrils formed from Aβ(1–42) peptide showed a lower unzipping force (~23 pN) than fibrils formed from Aβ(1–40) peptide (~33 pN) [99,100]. Unzipping experiments were also attempted on amyloids formed from Als cell adhesion proteins of a fungal pathogen, but in this case unzipping of mature fibrils was not possible. However, zipper interactions were detected between monolayers of Als proteins and an Als amyloid sequence attached to an AFM tip. The characteristic force signatures corresponded to the mechanical unzipping of β-sheet interactions formed between parallel Als proteins, and was about 30 pN [101].

The weak point of the above mentioned zipping experiments is that the measurements were based on nonspecific binding between tip and fibril. Therefore, the variability between individual measurements likely results from random and multiple attachment sites of the protein to the tip. The nanomechanical properties of human prion protein amyloid (huPrP90-231) were investigated using specific binding between the AFM tip and the fibril [102]. The protein was functionalized by replacing one amino acid for a

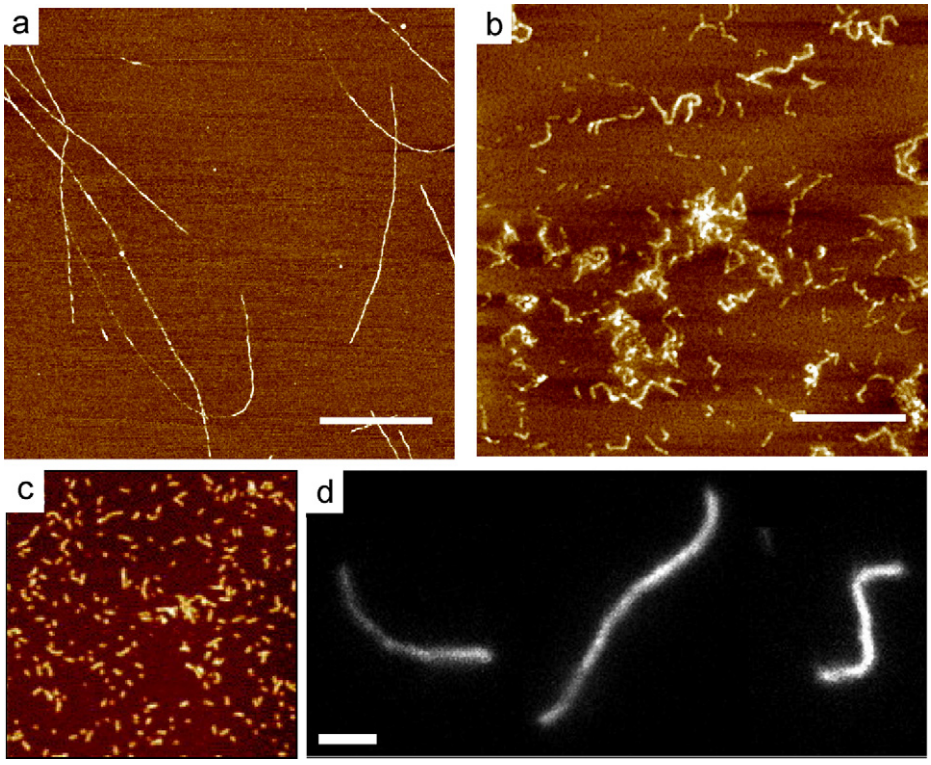

Fig. 10. AFM images of long, straight a. and worm-like b. β-lg amyloid fibrils. Scale bars are 500 nm. Reprinted with permission from VandenAkker et al. [60], J. Am. Chem. Soc. 2011, 133. c. Rod-like β-2-microglobulin amyloid fibrils. Image size is 1 × 1 μm. Reprinted with permission from Gosal et al. [91], J. Mol. Biol. 2005, 351. d. Fluorescence microscopy image of single yeast prion amyloid fibrils labeled with Thioflavin T. Scale bar is 2 μm. Reprinted with permission from Castro et al. [98], Biophys. J. 2011, 101.

cysteine, which is known to bind covalently with a gold-coated AFM tip. Again, force-extension curves showed elastic stretching for small retractions, characteristic of entropic stretching of a disordered peptide chain between the β-sheet core and the covalent attachment to the tip. At larger retractions of the tip, rupture occurred, which likely reflects the mechanical extraction of the prion protein from the core of the amyloid fibril. The force at which rupture took place, was 115 ± 5 pN at a tip retraction rate of 9.4 nN/s, and was dependent on the loading rate.

Even though amyloid fibrils are generally regarded mechanically strong, they do break under the influence of thermal forces. In fact, spontaneous fracture is thought to be a key feature of the kinetics of fibril growth, since fragmentation increases the number of free ends, thus enhancing the rate of fibril growth [2,103]. It has also been shown that amyloid fibrils break easily by elongational flow [104]. Whey protein isolate (WPI) amyloid fibrils already fracture at an elongational flow rate of only 8 s^{-1}, which is much lower than the flow rate where DNA strands break, which is close to 10,000 s^{-1}.

Table 1
Persistence lengths of straight and worm-like β-lg amyloid fibrils, measured using different techniques.

Reference	Morphology	Technique	Persistence length
VandenAkker [60], 2011	Straight	AFM	3820 nm ± 160
Adamcik [90], 2010	Straight	AFM	968–3240 nm
Jordens [96], 2011	Straight	AFM	2370 nm
Mudgal [93], 2009	Straight	TEM	788 nm
Veerman [95], 2002	Straight	TEM	1000 nm
Aymard [94], 1999	Straight	LS, SANS	600 nm
Sagis [37], 2004	Straight	Rheology	1600 nm ± 400
VandenAkker [60], 2011	Worm-like	AFM	92 nm ± 7
Jordens [96], 2011	Worm-like	AFM	29 nm
Mudgal [93], 2009	Worm-like	TEM	36 nm ± 12
Aymard [94], 1999	Worm-like	LS, SANS	38 nm

The fracture force estimated from these observations are 0.1 pN from the extensional flow experiment and 4 pN from the stability of fibrils against thermal force [104]. It is still unclear how these low fracture forces may be reconciled with the much higher fracture forces of 300–500 pN estimated from active nanomanipulation experiments of insulin fibrils [2]. It will be interesting to combine mechanical measurements with vibrational spectroscopy, to link the fracture strength to the underlying molecular structure, which may potentially depend on the peptide used as well as on the assembly conditions.

4.3. Extensibility

It was recently shown that the fundamental structural unit of several kinds of amyloid fibrils including Aβ is the β-helix structure [105–107]. The β-helix is a protein motif formed by the association of parallel β-strands in a helical pattern with either two or three faces (Fig. 11) [84]. The mechanical properties of this structure under tension and compression were studied with molecular dynamics (MD) simulations. The calculated maximum tensile force was 522 pN, while the maximum compressive force was much higher, namely 3150 pN. The simulations revealed that the β-helix structure is extremely extensible and can sustain tensile strains up to 800% without rupture of the covalently bonded protein backbone [84]. The model that was used only accounts for the core structure of certain amyloids, not including effects of side chains. It will be interesting to test by experiments the prediction that amyloid fibrils should be highly extensible.

4.4. Outlook

Although there is quite a large number of studies of the bending rigidity of single amyloid fibrils, most of these rely on AFM imaging

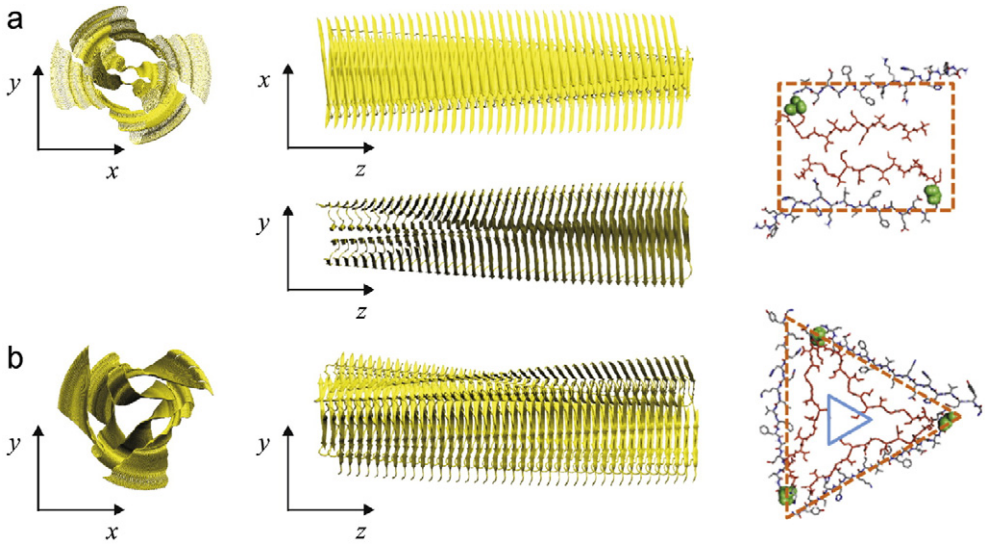

Fig. 11. Structures of a. twofold and b. threefold symmetric assemblies of Aβ(1–40) amyloid fibrils. Reprinted with permission from Xu et al. [86], Biophys. J. 2010, 98.

of fibrils deposited on a substrate and dried. It is unclear how surface immobilization and drying may affect the properties of the fibrils. Several techniques can be used to circumvent these experimental limitations. A promising method is to measure the thermal fluctuations of freely fluctuating amyloid fibrils with fluorescence microscopy, as was demonstrated for yeast prion amyloids [98]. Several studies have been reported of active mechanical manipulation of amyloid fibrils. In one study, amyloid fibrils were bent by an AFM tip, and in a few studies β-sheet segments were unzipped from fibrils by AFM. A promising technique to measure both the bending and stretch rigidity of amyloid fibrils is by a dual optical tweezers assay. As demonstrated in a recent study of microtubules and actin filaments, micrometer-sized beads can be attached to the two ends of a biopolymer and used as handles to stretch the biopolymer by two laser tweezers [108]. From the force-extension behavior, the persistence length of single, hydrated fibers could be determined based on well-controlled active experiments. Optical tweezers have also been used to measure the elastic moduli of individual fibers in networks of the blood clotting protein fibrin [109]. Micron-sized beads were attached to fibers after clot formation and trapped with optical tweezers. The bending and stretch rigidity of individual fibers was measured by applying an oscillatory displacement to the bead either orthogonally or tangentially to the fiber.

5. Microscopic properties of amyloid networks

For applications of amyloid fibrils in food products, tissue engineering, and materials sciences, the mechanical properties of networks are relevant. Network mechanics is determined by a combination of fibril mechanics and the spatial organization of fibrils and their interactions. The spatial organization of amyloid fibril networks depends on fibril rigidity: when the fibrils are long, thin, and rigid, they can form liquid crystalline phases or gels already at low concentrations [110]. The interactions between fibrils are not well-studied, but are thought to be highly dependent on the side chains on the surface of the fibrils, which can for instance confer a pH-dependent electrostatic charge to the fibrils [83]. Bulk rheology has been used to probe the mechanical properties of networks of amyloid fibrils [93,111,112]. The networks generally form weak viscoelastic gels. However, quantitative comparisons between rheology measurements and theory are still lacking, since the fibril morphology was not well-defined.

5.1. Rheological properties

Rheological properties relate to the flow properties of materials in response to an applied deformation. The most commonly used type of deformation is a shear deformation, where a material between two parallel plates is deformed by moving one of the plates while the other is kept stationary. Typically, one applies either a steady shear (constant shear rate) or an oscillatory shear of controlled strain amplitude and frequency, and measures the stress response. When the material is a Newtonian fluid such as water, the stress in a steady shear measurement is proportional to the applied shear rate with a constant of proportionality that is given by the steady-shear viscosity. The viscosity is independent of the shear rate. In contrast, polymeric materials are usually viscoelastic and non-Newtonian, with a viscosity that does depend on shear rate. Typically, the viscosity is constant at low strain rates, but decreases when the strain rate is raised, a response that is known as shear thinning. When the polymer material is elastic, a more suitable measurement is an oscillatory shear measurement, which measures the complex shear modulus G^*, which is the constant of proportionality between the stress and the strain. G^* is a complex quantity with a storage modulus G' that reflects the elastic stress response that is in-phase with the applied strain, and a loss modulus G'' that reflects the viscous stress response that is out-of-phase with the applied strain [110]. Until now, oscillatory measurements of amyloid networks have primarily focused on resolving the gelation time and critical percolation concentration of fibrils formed from food-related proteins including β-lg, bovine serum albumin (BSA) and ovalbumin at pH = 2 [37,112–114]. Steady shear measurements were used to measure the shear-rate dependence of the viscosity of suspensions of whey protein fibrils with lengths of several μm [111]. In all cases the suspensions were shear-thinning [111,113].

Oscillatory measurements have also been used to measure the influence of pH and ionic strength on gel strength. At pH = 3.35, the whey protein β-lg forms worm-like fibrils with a persistence length of 35 nm and a diameter of 5 nm [93]. The viscosity of these fibrillar networks was observed to increase with protein concentration. In the presence of NaCl, fibril networks remained predominantly elastic (with G' at least 10-fold higher than G'') up to ionic strengths of 100 mM, but became weaker and eventually fluid-like above 200 mM NaCl (Fig. 12) [115]. $BaCl_2$ and $MgCl_2$ caused a significantly

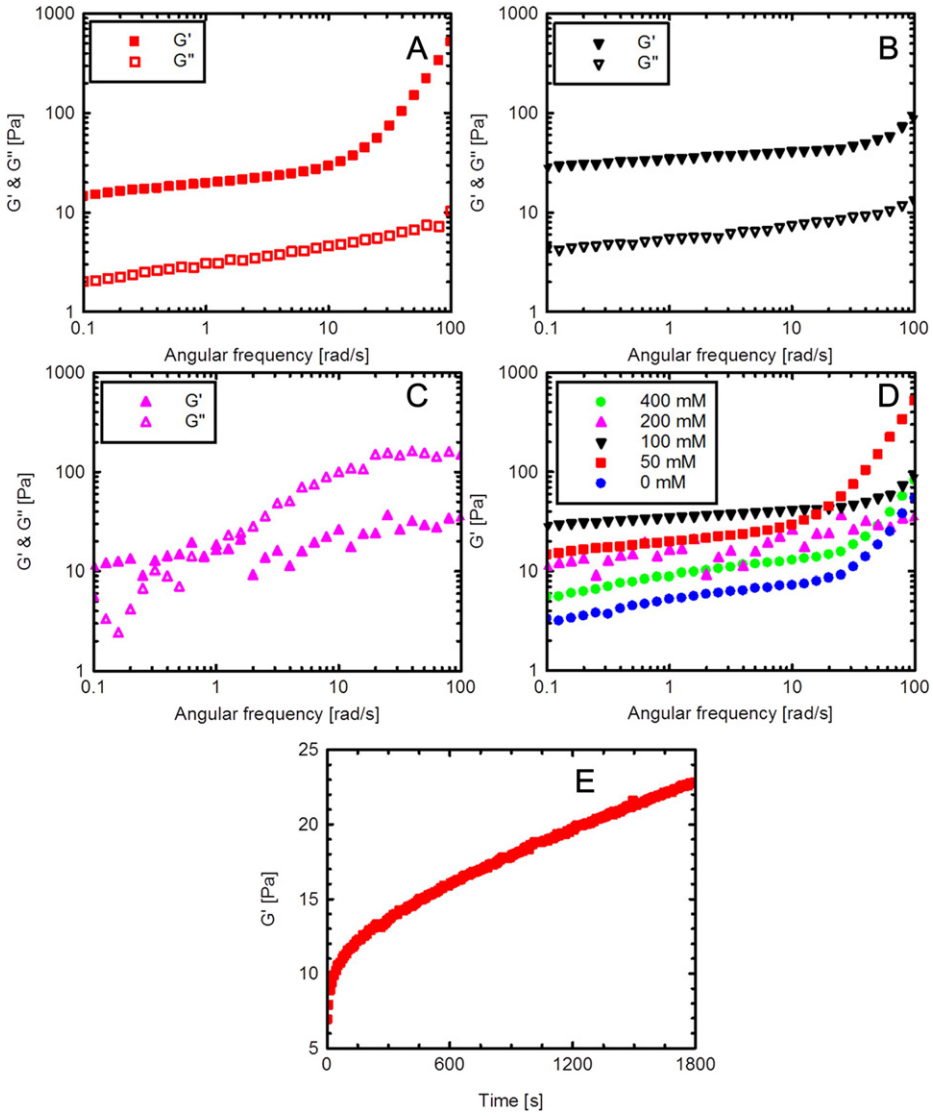

Fig. 12. Rheological characterization of 2% w/v β-lg protein fibrils at varying ionic strengths: A. 50 mM, B. 100 mM, and C. 200 mM NaCl. D. Storage modulus determined at different ionic strengths by frequency sweeps. E. Structural recovery behavior of the fibril gel prepared at the ionic strength of 50 mM as a function of time after destruction of the gel by a 100% oscillatory shear strain. Reprinted with permission from Ref. [115].

increased final viscosity of whey protein (WPI) gels compared to gels formed without salt [113]. Also monovalent salts increased the viscosity slightly compared to control fibrils formed without salt. All WPI fibrils formed in the presence of salt, showed a worm-like morphology, while fibrils formed without salt are generally long and straight. Frequency sweep and strain sweep experiments demonstrated that G' was relatively insensitive to added salt, but the loss modulus G'' was slightly higher with divalent salts than for samples without or with monovalent salts [113]. The viscosity depends on different parameters, including the volume fraction of fibrils, the fibril morphology and the interactions between fibrils. Because the effect of mono- and multivalent salts on these parameters was not determined, the mechanism behind the increase in viscosity is still not understood.

There are few rheological studies of amyloids other than whey proteins-related fibrils. Weak, solid-like behavior was also reported for hydrogels formed from amyloids of the Alzheimer related Aβ peptide, Aβ(16–20) formed at high concentrations (3% w/v) [112].

An alternative method to measure the rheology of soft polymeric materials is by microrheology (MR), which is a collection of techniques used to determine the local properties of a material from the motion of embedded, small tracer particles. The most popular MR technique is video particle tracking, where the thermally induced motions of the tracer particles are observed by optical microscopy [116]. Particle tracking is a convenient method to obtain a spatial map of variations in the viscoelastic properties of heterogenous samples [117]. An advantage of MR over bulk rheology is the possibility to use small sample volumes (down to 5 μL) and the possibility to determine the rheology over a broad frequency range. Particle tracking MR has been used to study the sol–gel transition in amyloid networks. Gels of β-lg fibrils were prepared at pH = 7 and room temperature by adding alcohol [116]. Under these conditions, wormlike fibrils are formed [118]. Latex particles with a diameter of 0.5 μm were used to observe the time evolution of network formation for β-lg concentrations at and above the critical gelation concentration of 4% w/v. In time, a shift from purely viscous to viscoelastic behavior was observed, indicative of fibril formation. Eventually, a solid gel was formed. Based on the mean squared displacement (MSD) of the probe particles, the elastic and loss moduli over a large frequency range could be

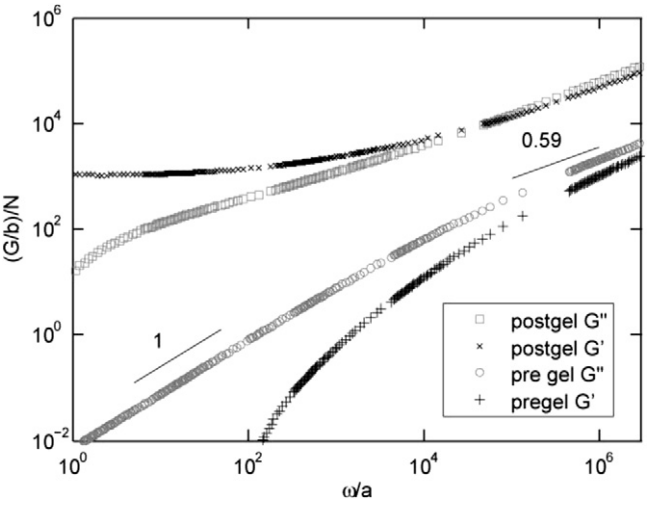

Fig. 13. Elastic and loss moduli of pre-gel (lower two curves) and post-gel (upper two curves) systems versus frequency, a and b are shift factors. For clarity, the postgel curves are shifted upward by a factor of 10^2, and only every fourth data point is plotted for each curve. The pregel curve shows viscous behavior at low frequencies (a slope of 1 for G''), while at high frequencies the moduli approach critical behavior and the power law exponent is 0.59, comparable to the MSD power law exponent at the gel point. Reprinted with permission from Corrigan et al. [116] Langmuir, 2009, 25. Copyright 2009 American Chemical Society.

calculated (Fig. 13). Similar experiments were also performed for β-lg amyloid fibrils formed by decreasing the pH to 2 and heating to 80 °C. Under these conditions, the fibrils that are formed are long and straight, and the critical concentration for gel formation was less than 3% w/v. The gels that were formed after about 100 min showed behavior typical of weak gels, with a plateau in G' that became more pronounced at longer incubation times up to 200 min [119].

5.2. Outlook

Particle tracking microrheology has a frequency range that is limited by the camera acquisition rate and also by the inherent localization error of ca. 20–50 nm in the particle position. These limitations can be overcome by using laser tweezers combined with quadrant photodiodes for sub-nanometer localization of probe particles embedded in a network. By using weak laser beams, the thermal fluctuations of the particles can be detected by laser-interferometry. As shown for actin networks and worm-like micelles, this method affords a wide frequency window of 0.1–100 kHz, giving at the same time access to network properties (below ~1 kHz) and single fibril properties (above ~10 kHz) [120,121]. Optical tweezers can also be used for active MR, where a probe particle is actively moved by a laser trap at controlled frequency and amplitude. This method in principle allows measurement of non-linear viscoelastic properties.

6. Conclusions/perspective

We have illustrated here how insights into amyloid chemistry and physics on different length scales ranging from the molecular to the macroscopic level can contribute to an improved understanding of amyloids and amyloid networks. The overarching goal of these efforts is to obtain a comprehensive understanding of the relation between secondary structure, amino acid distribution and fibril assembly on the one hand and morphology and mechanical properties of amyloids and networks thereof on the other hand. Network mechanics are necessarily a function of fibril mechanics, the architecture of networks, and interactions between fibrils. Fibrils mechanics are determined by the assembly and (core-) structure of fibrils, as well as interactions of single amino acids within the fibrils. It is evidently challenging to bridge the length scales from the molecular morphology, through single fibril mechanical properties, to the macroscopic rheological properties for these highly complex biopolymers, but some of the examples presented above demonstrate significant progress in this field. The recent development and application of advanced vibrational spectroscopic techniques to these complex biological systems show promise: several examples exist where a combination of techniques focusing on the properties of amyloids at different length scales was used. For example, the combination of vSFG and AFM allowed relating the persistence length of different assembly conditions to the global secondary structure composition of amyloids. The change in morphology and persistence length could be shown to be accompanied by a change in the secondary structure content of the amyloid samples. Sophisticated FT-IR and Raman spectroscopy can provide a comprehensive understanding of the secondary structure of amyloids [52,53,118], and may be combined with mechanical deformation in the same setup, as shown for other biopolymers [122]. The advent of several new vibrational spectroscopy techniques and microrheology approaches offers the possibility to interrogate macroscopic, mesoscopic and microscopic properties of amyloid fibrils.

Acknowledgment

This work is supported by NanoNextNL, a micro and nanotechnology consortium of the Government of the Netherlands and 130 partners, as well as part of the Industrial Partnership Programme (IPP) Bio(-Related) Materials (BRM) of the Stichting voor Fundamenteel Onderzoek der Materie (FOM), which is financially supported by the Nederlandse Organisatie voor Wetenschappelijk Onderzoek (NWO). The IPP BRM is co-financed by the Top Institute Food and Nutrition and the Dutch Polymer Institute.

References

[1] Vollrath F, Porter D. Polymer 2009;50(24):5623–32.
[2] Smith JF, Knowles TP, Dobson CM, Macphee CE, Welland ME. Proc Natl Acad Sci U S A 2006;103(43):15806–11.
[3] Knowles TP, Fitzpatrick AW, Meehan S, Mott HR, Vendruscolo M, Dobson CM, et al. Science 2007;318(5858):1900–3.
[4] Nyrkova IA, Semenov AN, Aggeli A, Bell M, Boden N, McLeish TCB. Eur Phys J B 2000;17(3):499–513.
[5] Dinca V, Kasotakis E, Catherine J, Mourka A, Ranella A, Ovsianikov A, et al. Nano Lett 2008;8(2):538–43.
[6] Scheibel T, Parthasarathy R, Sawicki G, Lin XM, Jaeger H, Lindquist SL. Proc Natl Acad Sci U S A 2003;100(8):4527–32.
[7] Hamada D, Yanagihara I, Tsumoto K. Trends Biotechnol 2004;22(2):93–7.
[8] Maji SK, Schubert D, Rivier C, Lee S, Rivier JE, Riek R. PLoS Biol 2008;6(2):240–51.
[9] Gelain F, Bottai D, Vescovi A, Zhang S. PLoS One 2006;1:e119.
[10] Hu KN, McGlinchey RP, Wickner RB, Tycko R. Biophys J 2011;101(9):2242–50.
[11] Berryman JT, Radford SE, Harris SA. Biophys J 2011;100(9):2234–42.
[12] Kodali R, Wetzel R. Curr Opin Struct Biol 2007;17(1):48–57.
[13] Sipe JD, Cohen AS. J Struct Biol 2000;130(2–3):88–98.
[14] Lin JC, Liu HL. Curr Drug Discov Technol 2006;3(2):145–53.
[15] Iconomidou VA, Hamodrakas SJ. Curr Protein Pept Sci 2008;9(3):291–309.
[16] Jahn TR, Makin OS, Morris KL, Marshall KE, Tian P, Sikorski P, et al. J Mol Biol 2010;395(4):717–27.
[17] Wiltzius JJ, Sievers SA, Sawaya MR, Cascio D, Popov D, Riekel C, et al. Protein Sci 2008;17(9):1467–74.
[18] Wetzel R, Shivaprasad S, Williams AD. Biochemistry 2007;46(1):1–10.
[19] Knowles TP, Smith JF, Craig A, Dobson CM, Welland ME. Phys Rev Lett 2006;96(23):238301.
[20] Guo S, Akhremitchev BB. Biomacromolecules 2006;7(5):1630–6.
[21] Pastor MT, Esteras-Chopo A, Lopez de la Paz M. Curr Opin Struct Biol 2005;15(1):57–63.
[22] Hamley IW. Angew Chem Int Ed Engl 2007;46(43):8128–47.

[23] Baldwin AJ, Bader R, Christodoulou J, MacPhee CE, Dobson CM, Barker PD. J Am Chem Soc 2006;128(7):2162–3.
[24] Hamedi M, Herland A, Karlsson RH, Inganas O. Nano Lett 2008;8(6):1736–40.
[25] Cellmer T, Bratko D, Prausnitz JM, Blanch HW. Trends Biotechnol 2007;25(6):254–61.
[26] Sinha S, Lieberburg I. Proc Natl Acad Sci U S A 1999;96(20):11049–53.
[27] Lansbury PT, Lashuel HA. Nature 2006;443(7113):774–9.
[28] Middleton CT, Marek P, Cao P, Chiu CC, Singh S, Woys AM, et al. Nat Chem 2012;4(5):355–60.
[29] Höppener JWM, Ahrén B, Lips CJM. N Engl J Med 2000;343(6):411–9.
[30] Kayed R, Head E, Thompson JL, McIntire TM, Milton SC, Cotman CW, et al. Science 2003;300(5618):486–9.
[31] Engel MFM, Khemtémourian L, Kleijer CC, Meeldijk HJD, Jacobs J, Verkleij AJ, et al. Proc Natl Acad Sci U S A 2008;105(16):6033–8.
[32] Butterfield SM, Lashuel HA. Angew Chem Int Ed 2010;49(33):5628–54.
[33] Kontopidis G, Holt C, Sawyer L. J Dairy Sci 2004;87(4):785–96.
[34] Gosal WS, Clark AH, Ross-Murphy SB. Biomacromolecules 2004;5(6):2420–9.
[35] Gosal WS, Clark AH, Ross-Murphy SB. Biomacromolecules 2004;5(6):2430–8.
[36] Arnaudov LN, de Vries R. Biomacromolecules 2006;7(12):3490–8.
[37] Sagis LM, Veerman C, van der Linden E. Langmuir 2004;20(3):924–7.
[38] Arnaudov LN, de Vries R. J Chem Phys 2007;126(14):145106.
[39] Padrick SB, Miranker AD. Biochemistry 2002;41(14):4694–703.
[40] Nanga RPR, Brender JR, Vivekanandan S, Ramamoorthy A. Biochim Biophys Acta Biomembr 2011;1808(10):2337–42.
[41] Nielsen JT, Bjerring M, Jeppesen MD, Pedersen RO, Pedersen JM, Hein KL, et al. Angew Chem Int Ed Engl 2009;48(12):2118–21.
[42] Kapurniotu A. Biopol Pept Sci 2001;60(6):438–59.
[43] Ono K, Yoshiike Y, Takashima A, Hasegawa K, Naiki H, Yamada M. J Neurochem 2003;87(1):172–81.
[44] Ehrnhoefer DE, Bieschke J, Boeddrich A, Herbst M, Masino L, Lurz R, et al. Nat Struct Mol Biol 2008;15(6):558–66.
[45] Cheynier V. Am J Clin Nutr 2005;81(1 Suppl.):223S–9S.
[46] Bieschke J, Russ J, Friedrich RP, Ehrnhoefer DE, Wobst H, Neugebauer K, et al. Proc Natl Acad Sci U S A 2010;107(17):7710–5.
[47] Fresco P, Borges F, Diniz C, Marques MP. Med Res Rev 2006;26(6):747–66.
[48] Manach C, Scalbert A, Morand C, Remesy C, Jimenez L. Am J Clin Nutr 2004;79(5):727–47.
[49] Shoval H, Lichtenberg D, Gazit E. Amyloid 2007;14(1):73–87.
[50] Azriel R, Gazit E. J Biol Chem 2001;276(36):34156–61.
[51] Necula M, Kayed R, Milton S, Glabe CG. J Biol Chem 2007;282(14):10311–24.
[52] Oboroceanu D, Wang LZ, Brodkorb A, Magner E, Auty MAE. J Agric Food Chem 2010;58(6):3667–73.
[53] Oboroceanu D, Wang LZ, Kroes-Nijboer A, Brodkorb A, Venema P, Magner E, et al. Int Dairy J 2011;21(10):823–30.
[54] Arnolds H, Bonn M. Surf Sci Rep 2010;65(2):45–66.
[55] Pettinger B, Schambach P, Villagomez CJ, Scott N. Annu Rev Phys Chem 2012;63:379–99.
[56] Bailo E, Deckert V. Chem Soc Rev 2008;37(5):921–30.
[57] Deckert-Gaudig T, Kammer E, Deckert V. J Biophotonics 2012;5(3):215–9.
[58] Bonn M, Bakker HJ, Ghosh A, Yamamoto S, Sovago M, Campen RK. J Am Chem Soc 2010;132(42):14971–8.
[59] Sovago M, Vartiainen E, Bonn M. J Chem Phys 2009;131(16):161107.
[60] vandenAkker CC, Engel MFM, Velikov KP, Bonn M, Koenderink GH. J Am Chem Soc 2011;133(45):18030–3.
[61] Fu L, Ma G, Yan ECY. J Am Chem Soc 2010;132(15):5405–12.
[62] Fu L, Liu J, Yan EC. J Am Chem Soc 2011;133(21):8094–7.
[63] Xiao D, Fu L, Liu J, Batista VS, Yan EC. J Mol Biol 2011.
[64] Engel MF, Vandenakker CC, Schleeger M, Velikov KP, Koenderink GH, Bonn M. J Am Chem Soc 2012;134(36):14781–8.
[65] Meng F, Abedini A, Plesner A, Verchere CB, Raleigh DP. Biochemistry 2010;49(37):8127–33.
[66] Diesner MO, Welle A, Kazanci M, Kaiser P, Spatz J, Koelsch P. Biointerphases 2011;6(4):171–9.
[67] Kurouski D, Deckert-Gaudig T, Deckert V, Lednev IK. J Am Chem Soc 2012;134(32):13323–9.
[68] Hamm P, Zanni MT. Concepts and methods of 2D infrared spectroscopy 2011.
[69] Cervetto V, Helbing J, Bredenbeck J, Hamm P. J Chem Phys 2004;121(12):5935–42.
[70] Bredenbeck J, Helbing J, Nienhaus K, Nienhaus GU, Hamm P. Proc Natl Acad Sci U S A 2007;104(36):14243–8.
[71] Strasfeld DB, Ling YL, Gupta R, Raleigh DP, Zanni MT. J Phys Chem B 2009;113(47):15679–91.
[72] Shim SH, Zanni MT. Phys Chem Chem Phys 2009;11(5):748–61.
[73] Wang L, Middleton CT, Singh S, Reddy AS, Woys AM, Strasfeld DB, et al. J Am Chem Soc 2011;133(40):16062–71.
[74] Baiz CR, Peng CS, Reppert ME, Jones KC, Tokmakoff A. Analyst 2012;137(8):1793–9.
[75] Zhuang W, Hayashi T, Mukamel S. Angew Chem Int Ed Engl 2009;48(21):3750–81.
[76] Luca S, Yau WM, Leapman R, Tycko R. Biochemistry 2007;46(47):13505–22.
[77] Paravastu AK, Leapman RD, Yau WM, Tycko R. Proc Natl Acad Sci U S A 2008;105(47):18349–54.
[78] Shim SH, Gupta R, Ling YL, Strasfeld DB, Raleigh DP, Zanni MT. Proc Natl Acad Sci U S A 2009;106(16):6614–9.
[79] Strasfeld DB, Ling YL, Shim SH, Zanni MT. J Am Chem Soc 2008;130(21):6698–9.
[80] Ling YL, Strasfeld DB, Shim SH, Raleigh DP, Zanni MT. J Phys Chem B 2009;113(8):2498–505.
[81] Meng F, Abedini A, Plesner A, Middleton CT, Potter KJ, Zanni MT, et al. J Mol Biol 2010;400(3):555–66.
[82] Cao P, Meng F, Abedini A, Raleigh DP. Biochemistry 2010;49(5):872–81.
[83] Knowles TP, Buehler MJ. Nat Nanotechnol 2011;6(8):469–79.
[84] Keten S, Buehler MJ. Comput Meth Appl Mech Eng 2008;197(41–42):3203–14.
[85] Jones OG, Mezzenga R. Soft Matter 2012;8(4):876–95.
[86] Xu Z, Paparcone R, Buehler MJ. Biophys J 2010;98(10):2053–62.
[87] Mucke N, Klenin K, Kirmse R, Bussiek M, Herrmann H, Hafner M, et al. PLoS One 2009;4(11):e7756.
[88] Brangwynne CP, Koenderink GH, Barry E, Dogic Z, MacKintosh FC, Weitz DA. Biophys J 2007;93(1):346–59.
[89] Relini A, Torrassa S, Ferrando R, Rolandi R, Campioni S, Chiti F, et al. Biophys J 2010;98(7):1277–84.
[90] Adamcik J, Jung JM, Flakowski J, De Los Rios P, Dietler G, Mezzenga R. Nat Nanotechnol 2010;5(6):423–8.
[91] Gosal WS, Morten IJ, Hewitt EW, Smith DA, Thomson NH, Radford SE. J Mol Biol 2005;351(4):850–64.
[92] Sachse C, Grigorieff N, Fandrich M. Angew Chem Int Ed 2010;49(7):1321–3.
[93] Mudgal P, Daubert CR, Foegeding EA. Food Hydrocolloids 2009;23(7):1762–70.
[94] Aymard P, Nicolai T, Durand D, Clark A. Macromolecules 1999;32(8):2542–52.
[95] Veerman C, Ruis H, Sagis LM, van der Linden E. Biomacromolecules 2002;3(4):869–73.
[96] Jordens S, Adamcik J, Amar-Yuli I, Mezzenga R. Biomacromolecules 2011;12(1):187–93.
[97] Ban T, Hamada D, Hasegawa K, Naiki H, Goto Y. J Biol Chem 2003;278(19):16462–5.
[98] Castro CE, Dong J, Boyce MC, Lindquist S, Lang MJ. Biophys J 2011;101(2):439–48.
[99] Kellermayer MS, Grama L, Karsai A, Nagy A, Kahn A, Datki ZL, et al. J Biol Chem 2005;280(9):8464–70.
[100] Karsai A, Martonfalvi Z, Nagy A, Grama L, Penke B, Kellermayer MS. J Struct Biol 2006;155(2):316–26.
[101] Alsteens D, Ramsook CB, Lipke PN, Dufrene YF. ACS Nano 2012;6(9):7703–11.
[102] Ganchev DN, Cobb NJ, Surewicz K, Surewicz WK. Biophys J 2008;95(6):2909–15.
[103] Tanaka M, Collins SR, Toyama BH, Weissman JS. Nature 2006;442(7102):585–9.
[104] Kroes-Nijboer A, Venema P, Baptist H, van der Linden E. Langmuir 2010;26(16):13097–101.
[105] Govaerts C, Wille H, Prusiner SB, Cohen FE. Proc Natl Acad Sci U S A 2004;101(22):8342–7.
[106] Kishimoto A, Hasegawa K, Suzuki H, Taguchi H, Namba K, Yoshida M. Biochem Biophys Res Commun 2004;315(3):739–45.
[107] Perutz MF, Finch JT, Berriman J, Lesk A. Proc Natl Acad Sci U S A 2002;99(8):5591–5.
[108] van Mameren J, Vermeulen KC, Gittes F, Schmidt CF. J Phys Chem B 2009;113(12):3837–44.
[109] Collet JP, Shuman H, Ledger RE, Lee S, Weisel JW. Proc Natl Acad Sci U S A 2005;102(26):9133–7.
[110] Loveday SM, Rao MA, Creamer LK, Singh H. J Food Sci 2009;74(3):R47–55.
[111] Akkermans C, van der Goot AJ, Venema P, van der Linden E, Boom RM. Food Hydrocolloids 2008;22(7):1315–25.
[112] Krysmann MJ, Castelletto V, Kelarakis A, Hamley IW, Hule RA, Pochan DJ. Biochemistry 2008;47(16):4597–605.
[113] Loveday SM, Su JH, Rao MA, Anema SG, Singh H. Int Dairy J 2012;26(2):133–40.
[114] Veerman C, de Schiffart G, Sagis LM, van der Linden E. Int J Biol Macromol 2003;33(1–3):121–7.
[115] Bolisetty S, Harnau L, Jung JM, Mezzenga R. Biomacromolecules 2012;13(10):3241–52.
[116] Corrigan AM, Donald AM. Langmuir 2009;25(15):8599–605.
[117] Valentine MT, Kaplan PD, Thota D, Crocker JC, Gisler T, Prud'homme RK, et al. Phys Rev E Stat Nonlin Soft Matter Phys 2001;64(6 Pt 1):061506.
[118] Gosal WS, Clark AH, Ross-Murphy SB. Biomacromolecules 2004;5(6):2408–19.
[119] Corrigan AM, Donald AM. Eur Phys J E Soft Matter 2009;28(4):457–62.
[120] Koenderink GH, Atakhorrami M, MacKintosh FC, Schmidt CF. Phys Rev Lett 2006;96(13):138307.
[121] Atakhorrami M, Mizuno D, Koenderink GH, Liverpool TB, MacKintosh FC, Schmidt CF. Phys Rev E Stat Nonlin Soft Matter Phys 2008;77(6 Pt 1):061508.
[122] Boulet-Audet M, Vollrath F, Holland C. Phys Chem Chem Phys 2011;13(9):3979–84.

Michael Schleeger received his diploma in chemistry from the University of Bonn (2004). For his Ph.D. thesis, he joined the group of Joachim Heberle at Bielefeld University, where he received his Ph.D. degree in 2009. After 2 years of postdoctoral research in the Department of Physics at the FU Berlin, he joined the group of Prof. Mischa Bonn at the Max-Planck Institute for Polymer research in Mainz as a research fellow in 2012. His current research focus is on the structure and interactions of amyloids based on vibrational spectroscopy, in particular sum frequency generation spectroscopy.

Corianne van den Akker obtained her Master's degree in Biomedical Engineering from the University of Twente, The Netherlands in 2010. She is currently studying for a PhD with Prof. Gijsje Koenderink at FOM Institute AMOLF in Amsterdam, with research orientated towards the mechanical properties and molecular conformation of amyloid fibrils.

Dr. Tanja Deckert-Gaudig works as a postdoc in the research group of Prof. V. Deckert at the Institute of Photonic Technology in Jena. She obtained her Ph.D. in Organic Chemistry in 1997 with Prof. S. Hünig at the University of Würzburg. After a maternal leave she started working on TERS with Prof. Deckert at the University of Dresden in 2002, followed by the Institute of Analytical Sciences in Dortmund. Since 2009 she works in Jena, where her main interest is the structural elucidation of biopolymers on the nanoscale by TERS.

Prof. Volker Deckert holds a joint position at the Institute of Physical Chemistry at the University of Jena, Germany and the Institute of Photonic Technology, also in Jena. He obtained his Diploma and Ph.D. from the University of Würzburg, Germany, working on difference-Raman spectroscopy. As a postdoc at the University of Tokyo and the Kanagawa Academy of Science in Kawasaki, he worked on non-linear and time-resolved laser spectroscopy of photo-induced isomerisation reactions. During his habilitation at the ETH Zurich he started working on the development of high spatial resolution techniques for Raman spectroscopy. This topic was the basis of his next positions at the TU Dresden, ISAS Dortmund and now in Jena, where he in particular explores the possibilities of the technology to investigate structural changes of bio-related compounds with nanometer resolution.

Dr. Krassimir Velikov is a Science/Team Leader in Unilever R&D Vlaardingen. He received his PhD from the University of Utrecht, The Netherlands. His main research interests cover topics of soft-condensed matter, self-assembly, colloid and interface science of dispersions (e.g. suspensions, foams, emulsions) and their uses to control product functionality (e.g. stability, appearance, texture), physical-chemistry of digestion, and formulation and delivery of functional ingredients. He is an adjunct assistant professor in the Soft Condensed Matter group at the Debye Institute for NanoMaterials Science, Utrecht University and a special adjunct associate professor in the Department of Chemical and Biomolecular Engineering in the College of Engineering, North Carolina State University (USA). He is a Program Director of Molecular Structure of Food program in NanoNextNL.

Gijsje Koenderink received her Ph.D. from Utrecht University in 2003 in the area of physical and colloid chemistry. She conducted postdoctoral research at the VU University (Amsterdam) and Harvard University (Cambridge MA) on biophysical properties of cytoskeletal biopolymers. She joined the FOM Institute AMOLF in Amsterdam as a group leader in 2006, where she started the group "Biological Soft Matter". Her research interests focus on the structural and mechanical properties of biopolymers, the non-equilibrium properties of the cellular cytoskeleton, and cellular mechanosensing.

Mischa Bonn (January 25, 1971, The Netherlands) received his PhD in 1996 for work resulting from a collaboration between the Technical University of Eindhoven and the FOM Institute for Atomic and Molecular Physics, AMOLF. After post-doctoral work at the Fritz-Haber Institute in Berlin and Columbia University in New York, Mischa worked at the chemistry department at Leiden University (1999–2004), before moving to AMOLF (2004) as head of the "Biosurface Spectroscopy" group. Mischa received 2009 the Gold Medal from the Royal Dutch Chemical Society. In 2011 Mischa was appointed as one of the Directors of the Max Planck Institute for Polymer Research in Mainz. His research is centered around laser-based vibrational spectroscopies, specifically surface and THz spectroscopies and CARS microscopy.